ADVANCING EARTH AND SPACE SCIENCES

Tectonics

RESEARCH ARTICLE

10.1029/2025TC009200

Key Points:

- Transverse zones are long-lived structures reactivated multiple times in fold-and-thrust belts
- Tectonic evolution of the Central Southern Alps from Late Triassic-Jurassic rifting to Cretaceous-Late Miocene shortening
- Structural, stratigraphic constraints and U–Pb geochronology on fault-related carbonates

Supporting Information:

Supporting Information may be found in the online version of this article.

Correspondence to:

A. Fiorini,
andrea.fiorini@uniroma1.it

Citation:

Fiorini, A., Tavani, S., Aldega, L., Kylander-Clark, A., Rocca, M., Zanchetta, S., et al. (2026). Origin, recurrent reactivations, and tectonic role of transverse zones in thrust-and-fold belts: The Central Southern Alps (Italy). *Tectonics*, *45*, e2025TC009200. https://doi.org/10.1029/2025TC009200

Received 16 SEP 2025
Accepted 25 JUN 2026

Author Contributions:

Conceptualization: A. Fiorini, L. Aldega, M. Rocca, S. Zanchetta, A. Zanchi, E. Carminati
Data curation: A. Fiorini, A. Kylander-Clark
Formal analysis: A. Fiorini, A. Kylander-Clark, M. Rocca, A. Zanchi
Funding acquisition: A. Fiorini, L. Aldega, S. Zanchetta, E. Carminati
Investigation: A. Fiorini, S. Tavani, A. Kylander-Clark, M. Rocca, S. Zanchetta, A. Zanchi, E. Carminati
Methodology: A. Fiorini, A. Kylander-Clark, M. Rocca
Project administration: E. Carminati
Resources: A. Kylander-Clark
Supervision: E. Carminati
Validation: S. Tavani

Origin, Recurrent Reactivations, and Tectonic Role of Transverse Zones in Thrust-and-Fold Belts: The Central Southern Alps (Italy)

A. Fiorini[1], S. Tavani[2,3], L. Aldega[1], A. Kylander-Clark[4], M. Rocca[5], S. Zanchetta[5], A. Zanchi[5], and E. Carminati[1]

[1]Earth Science Department, Sapienza Università di Roma, Roma, Italy, [2]DST, Università Degli Studi di Firenze, Firenze, Italy, [3]c.o. Dipartimento di Scienze Della Terra, National Research Council (CNR), IGAG, Sapienza Università di Roma, Roma, Italy, [4]Department of Earth Science, University of California, Santa Barbara, CA, USA, [5]Department of Earth and Environmental Science, Università degli Studi di Milano Bicocca, Milan, Italy

Abstract Transverse zones (TZs) in fold-and-thrust belts typically comprise strike-slip to transpressional faults and related folds, oriented sub-parallel to the regional shortening direction. These zones are typically associated with inherited faults or lateral stratigraphic changes, which promote strain partitioning, stress rotation, and kinematic decoupling between adjacent blocks. In the Central Southern Alps (CSA), transverse zones sub-parallel to the N–S shortening direction originated as pre-orogenic rift-related faults, later reactivated during the Alpine orogeny under compressional regimes. Their structural complexity has long been recognized, but no systematic absolute dating has constrained their long-term evolution and reactivation history. To address this gap, we combine geological mapping, multi-scale structural analysis, and U–Pb geochronology on syn-tectonic carbonates from TZs and major thrust faults in the Lecco area to reconstruct their structural evolution within the Alpine thrust system. We infer a pre-orogenic origin for N–S TZs and some E–W striking faults linked to rift-related extensional tectonics active during the Late Norian and Early–Middle Jurassic times. U–Pb ages provide new insights into the Early Cretaceous-Miocene syn-orogenic evolution of the Central Southern Alps. During this interval, rift-inherited N–S faults were episodically reactivated in strike-slip mode under N–S shortening for nearly 100 Ma. We discuss how the TZs influence the build-up of the belt, promoting along-strike strain partitioning, acting as lateral connectors of thrusts and contributing to shortening accommodation when oblique to the maximum horizontal compression.

1. Introduction

Fold-and-thrust belts typically exhibit complex 3D architectures along strike, where strike-parallel structures are segmented by transverse zones (TZs). These zones consist of strike-slip and/or transpressive faults and/or folds, oriented at a low angle to the regional shortening direction (Thomas, 1990). The location of TZs is commonly controlled by inherited structures, including basement faults (e.g., Godin et al., 2019; Krabbendam & Leslie, 2010; Torres Carbonell et al., 2013), usually displacing the overlying sedimentary cover (e.g., Bertotti, 1991; Paulsen & Marshak, 1998, 1999; Schönborn, 1992; Zanchi et al., 2012), ancestral transform faults (e.g., Feriozzi et al., 2025), zones of spatial overlap between rift segments forming complex accommodation domains (e.g., Lescoutre et al., 2021), zones of stratigraphic thickness and/or facies variation (e.g., Soto et al., 2002; Woodward et al., 1988), and heterogeneities in lower crustal rheology (e.g., Malekzade et al., 2016). TZs may laterally connect thrust faults, accommodating deformation by acting as lateral ramps and/or transfer faults (García & Jiménez, 2016; Schönborn, 1992; Thomas & Bayona, 2002; Zanchi et al., 2012). In these cases, thrusting and folding overprint the inherited structural architecture, frequently truncating, displacing and folding laterally juxtaposed different rocks in the hanging wall and footwall of pre-existing extensional systems. This structural overprint may complicate the recognition of both the primary pre-thrusting architecture and the thrust system. In detail, during the development of a fold-and-thrust belt, pre-orogenic cross-strike structures can either be passively transported and deformed by later thrust faults (e.g., Alavi, 2007), or actively influence the propagation of contractional structures, cutting across the entire belt and segmenting it into discrete structural blocks (Schönborn, 1992; Schwartz et al., 2024). The study of TZs, fundamental to a full understanding of mountain building processes, is therefore challenging because it requires a complete reconstruction of the pre-orogenic tectono-stratigraphic setting and of the impact of inherited features on the geometry of thrusts and along-strike strain partitioning.

Visualization: A. Fiorini, S. Tavani
Writing – original draft: A. Fiorini
Writing – review & editing: S. Tavani, L. Aldega, A. Kylander-Clark, M. Rocca, S. Zanchetta, A. Zanchi, E. Carminati

Polyphase tectonic activity of TZs has been proposed (e.g., Castellarin et al., 2006; Glen & Walshe, 1999; Zanchi et al., 2012), but radiometric ages supporting this hypothesis are generally scarce (e.g., Pleuger et al., 2012, for the Alps, and references therein). To address this issue, we investigate TZs, inherited structures and thrust faults of the western sector of the Central Southern Alps (CSA), specifically in the Lecco area (Figure 1). The CSA represent a retro-belt where transverse zones (TZs) influence shortening style across-strike (Schönborn, 1992). Syn-thrusting and polyphase tectonic activity of TZs within the belt has been documented in previous studies (e.g., Schönborn, 1992; Zanchi et al., 1988, 2012). A key example in the CSA is the Giudicarie Line, which originated as an Early Jurassic normal fault and was subsequently reactivated during multiple orogenic phases as a left-lateral transpressional fault (Bertotti et al., 1993; Castellarin et al., 2006; Picotti et al., 1995; Pomella et al., 2012; Prosser, 1998; Viola et al., 2001). In the Eastern Southern Alps (ESA), TZs remain tectonically active to date, as evidenced by moderate seismicity (Carulli & Slejko, 2009; Zampieri, 2000; Zampieri et al., 2021).

Regarding the TZs of the CSA, several key questions are still open: (a) what is their origin, including the role of structural inheritance? (b) When and how were they reactivated during Alpine evolution and later tectonic stages? (c) What is the role of TZs during shortening?

To answer these questions, we combine paleogeographic reconstructions, structural-geological analysis (from regional to microscale) and U–Pb dating of syn-tectonic carbonates in the western sector of the CSA (Lecco area, Figures 1b, 2, 3). We propose that TZs developed along pre-orogenic rift-related extensional faults and that they were reactivated multiple times from rifting to late orogenic stages. Our findings offer a valuable framework for interpreting the origin, evolution and structural role of TZs in other fold-and-thrust belts (e.g., Bayona et al., 2003; Paulsen & Marshak, 1999; Schmidt & O'Neill, 1982; Smeraglia et al., 2022; Ustaszewski & Schmid, 2006).

2. Geological Setting

2.1. The Central Southern Alps

The south-verging Central Southern Alps (CSA) are part of the Alpine retrobelt (Carminati & Doglioni, 2012; Schmid et al., 2004), which developed due to the convergence and collision between the Adria and European plates at the expense of the intervening Alpine Tethys oceanic domain (Dal Piaz et al., 2003). This belt is located south of the Periadriatic Lineament (or Insubric line; Schmid et al., 1989; Figure 1a), is composed of rocks belonging to the Adria plate (Handy et al., 2010), and strikes approximately E–W, from the Como area to the Giudicarie Line (Figure 1b). The CSA developed since Cretaceous times as a thick-skinned fold-and-thrust belt (Carminati et al., 1997; Castellarin et al., 1992; Laubscher, 1985; Schmid et al., 1996; Schönborn, 1992; Schumacher et al., 1997; Zanchetta et al., 2012, 2015; Zanchi et al., 1990). The uppermost (and northernmost) thrust sheet consists of pre-Alpine basement rocks, which overthrusted Upper Permian–Lower Triassic successions along the Orobic-Gallinera Thrust during the Late Cretaceous and Paleocene–Eocene (Blom & Passchier, 1997; Carminati et al., 1997; Zanchetta et al., 2011; Figure 1b). The footwall of the Orobic-Gallinera Thrust is characterized by WSW–ENE-elongated basement-cored anticlines (Orobic Anticlines; de Sitter & de Sitter-Koomans, 1949; Schönborn, 1992; Figure 1b). The Orobic Anticlines are bounded to the south by a S-dipping backthrust (Valtorta-Valcanale Fault [VVF], Zanchetta et al., 2015; Figure 1b). South of the VVF, thrust sheets mainly involve the Lower-Triassic-Upper Cretaceous sedimentary cover. There, deformation is mainly dominated by south-vergent thrusts (Figures 1b, 2a, and 4a). These thrust systems define tectonic units composed of (a) Anisian-Ladinian formations, (b) Norian formations, and (c) Upper Triassic to Upper Cretaceous formations (Figures 1b, 2b, and 3a). Décollement horizons are located within mechanically weak stratigraphic levels, including the Lower Triassic, Carnian, and upper Norian-Rhaetian intervals (Figure 4a). The geometry and deformation style of the thrust system vary significantly along strike. This lateral variability is largely influenced by N–S oriented, subvertical TZs (Schönborn, 1992; Zanchi et al., 2012; Figures 1b, 2b, 3a, and 4b). Stratigraphic constraints suggest that these structures formed as normal faults during Late Triassic and Jurassic rifting events (Berra & Carminati, 2010). These N–S oriented normal faults, along with coeval E–W striking faults, controlled the distribution of Upper Triassic and Jurassic facies and sediment thickness, and caused the lateral juxtaposition of pre-rift sedimentary successions with contrasting rheological properties (Bernoulli, 2007; Berra & Carminati, 2010; Bertotti, 1991).

Another major structure of the area, marking the southernmost exposure of the Upper Triassic-Upper Cretaceous succession, corresponds to the "Flessura Pedemontana" (Desio, 1929; Figures 1b, 2, 3a, and 4a), a S-verging kink anticline previously interpreted as an out-of-sequence structure (Bersezio et al., 1993; Fantoni et al., 2004;

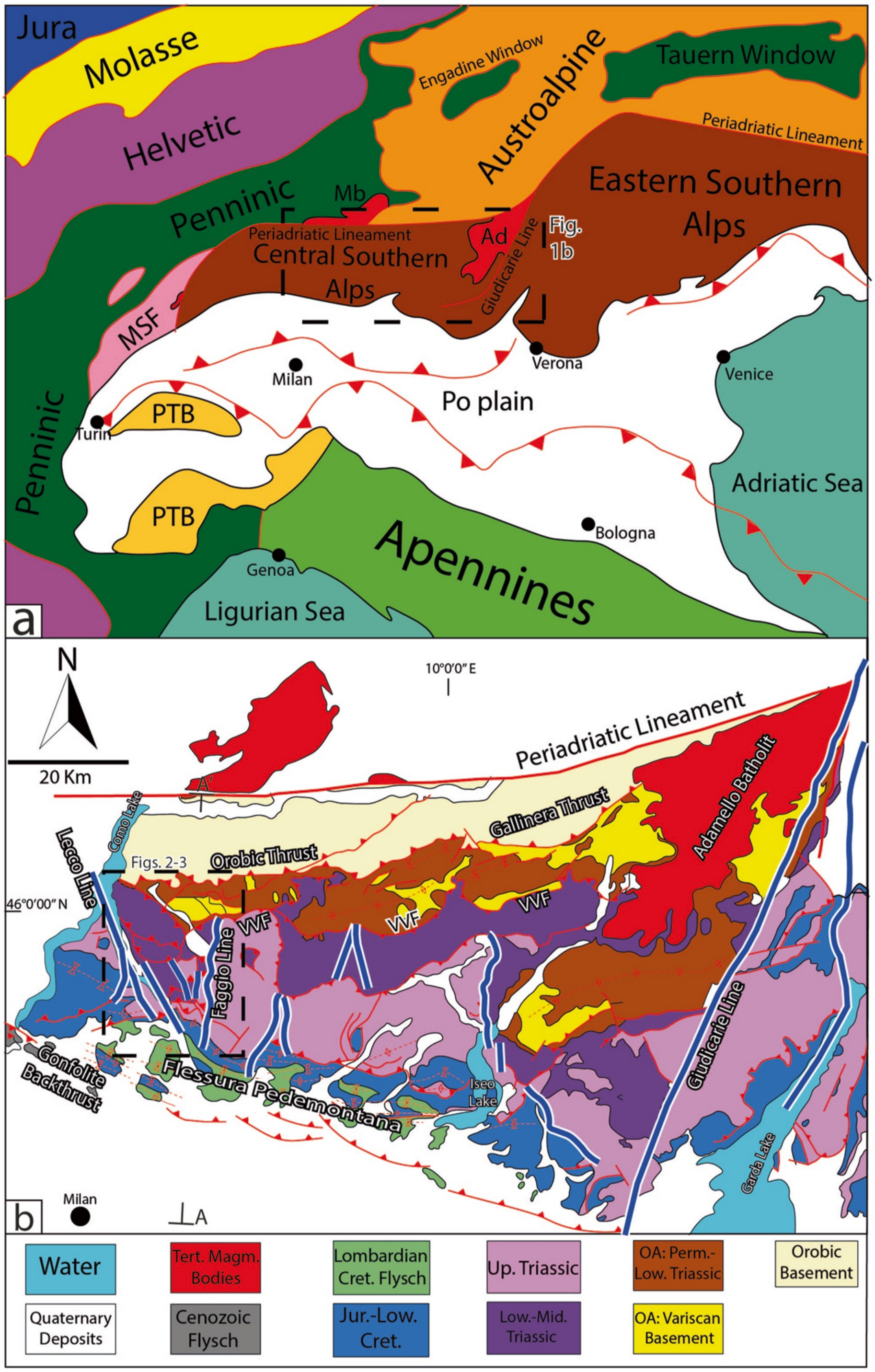

Figure 1. (a) Paleogeographic-structural domains of the Alps (modified from Schmid et al., 2004; Zanchi et al., 2012) PTB: Piedmont Tertiary Basin, MSF: Margna-Sesia Fragment; Mb: Masino-Bregaglia pluton; Ad: Adamello Pluton.
(b) Simplified geological map of the Central Southern Alps; the main transverse zones are highlighted in blue (modified from Schönborn, 1992; Zanchetta et al., 2015). VVF: Valtorta-Valcanale Fault, OA: Orobic Anticlines. The tip points of the geological cross-section A-A′ in Figure 4a are highlighted.

Schönborn, 1992; Schumacher et al., 1997; Figure 4a). South of this structure, Upper Cretaceous-Eocene foredeep units form a WNW–ESE elongated belt extending from the foothills of the Lecco area to the Iseo Lake (Bersezio & Fornaciari, 1987; Forcella et al., 2000; Figures 1b, 2, and 3a). These units were thrust and deformed

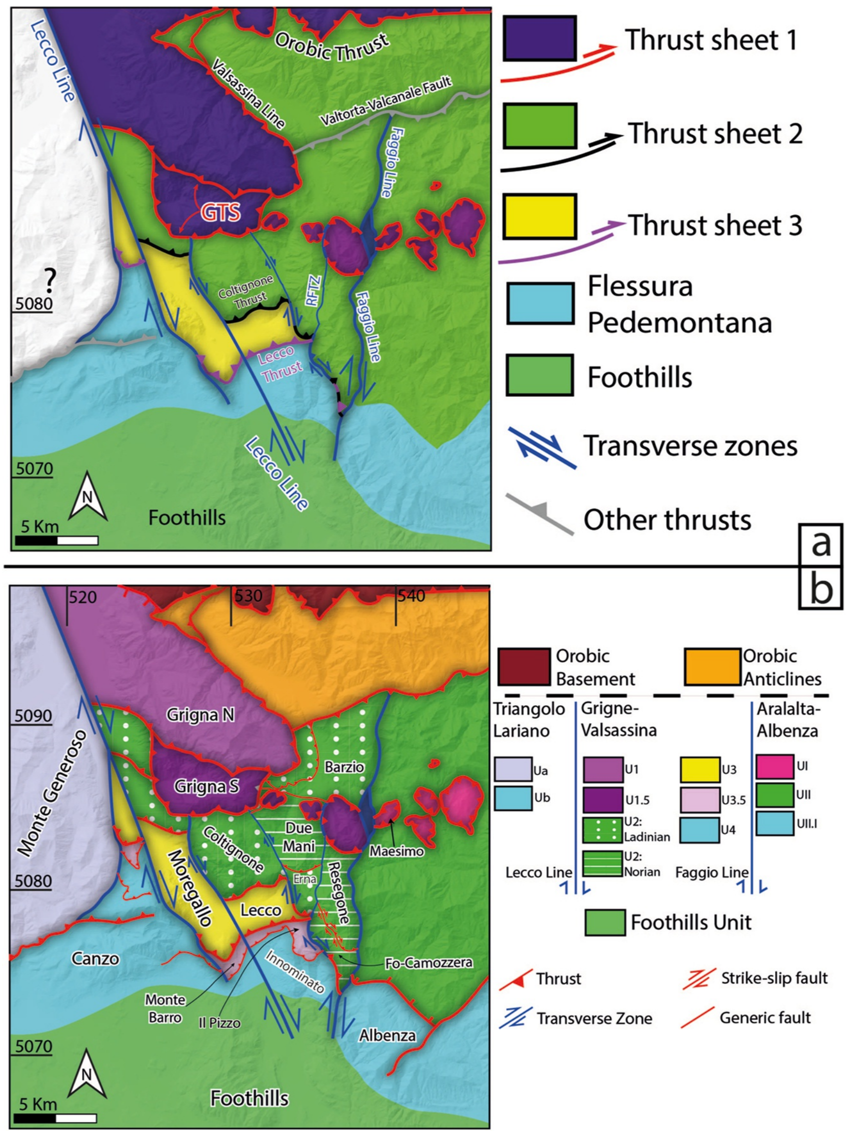

Figure 2. (a) Tectonic map of the study area (modified after Schönborn, 1992). The main thrust sheets are illustrated. GTS: Grigne Thrust System; RFTZ: Riva Foppa-Fo Transverse Zone. (b) Tectono-structural map of the study area (modified after Schönborn, 1992). The tectonic units recognized in the three sectors are shown from top to bottom and indicated as Ua-b, U1-4, and UI-II.b.

southward during the Cenozoic (Pieri & Groppi, 1981; Bersezio et al., 2001; Fantoni et al., 2004; Figure 4a) and unconformably overlain by the Oligocene-Miocene Gonfolite clastic wedge, which was back-thrust onto the Mesozoic units during the Late Miocene (Gonfolite backthrust, Bernoulli et al., 1989). Further south, contractional structures buried beneath Pliocene-Pleistocene sediments of the Po-Plain define the so-called Milano Belt (Fantoni et al., 2004; Laubscher, 1985; Roeder, 1992; Figure 4a) and are locally considered to be still active (Bresciani & Perotti, 2014; Zanchi et al., 2022).

2.2. Tectono-Stratigraphic Setting of the Study Area

The stratigraphic succession exposed in the study area (Figure 3b) starts with Lower Permian clastic, volcanic and volcaniclastic deposits (overlying basement rocks) and Upper Permian fluvial deposits (Casati & Gnaccolini, 1967). The thickness and facies of Permian deposits are strongly influenced by E–W striking Early Permian normal faults (Assereto & Casati, 1965; Locchi et al., 2022; Pohl et al., 2018; Schaltegger & Brack, 2007; Zanchi et al., 2019). A Lower Triassic marine transgression led to the deposition of quartzarenites, marls, limestones,

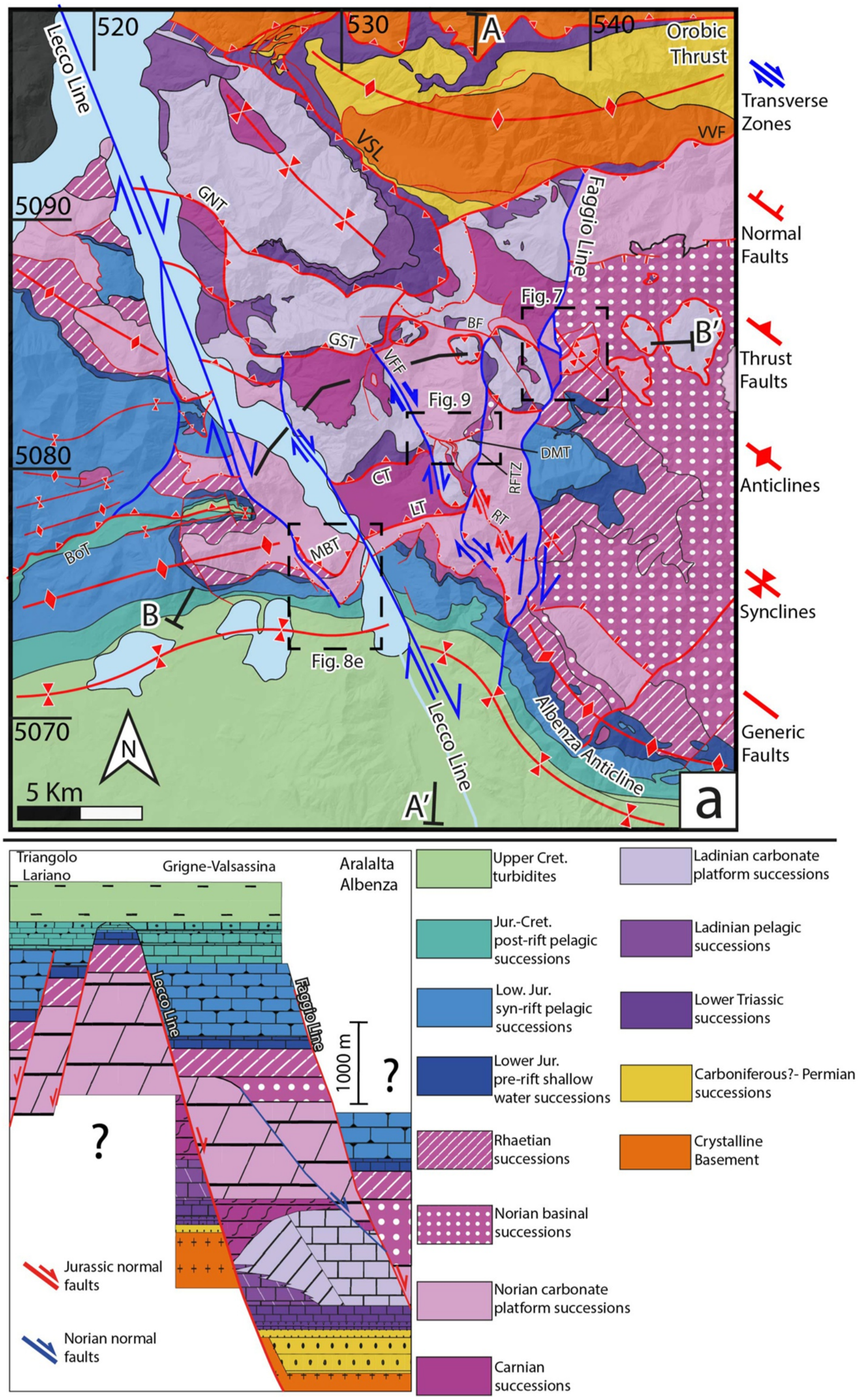

Figure 3. (a) Geological map of the study area (modified after Bersezio et al., 2014; Gaetani et al., 2012; Jadoul, 1994; Michetti et al., 2012; Regione Lombardia, 2010; Schönborn, 1992); BF: Balisio Fault; BoT: Monte Bollettone Thrust; CT: Coltignone Thrust; DMT: Due Mani Thrust; RFTZ: Riva Foppa—Fo Transverse Zone; GNT: Grigna Nord Thrust; GST: Grigna Sud Thrust; LT: Lecco Thrust; MBT: Monte Barro Thrust; RT: Resegone Thrust; VSL: Valsassina Line; VFF: Val Fontana Fault; VVF: Valtorta-Valcanale Fault. The terminal points of the geological cross-sections A-A′ (full length in Figure 1b) and B-B′ of Figure 4 are shown. (d)Tectono-stratigraphic scheme of the study area, showing the pre-orogenic relationships between faults and sedimentary units; the unit colors in the legend are the same used in the geological map.

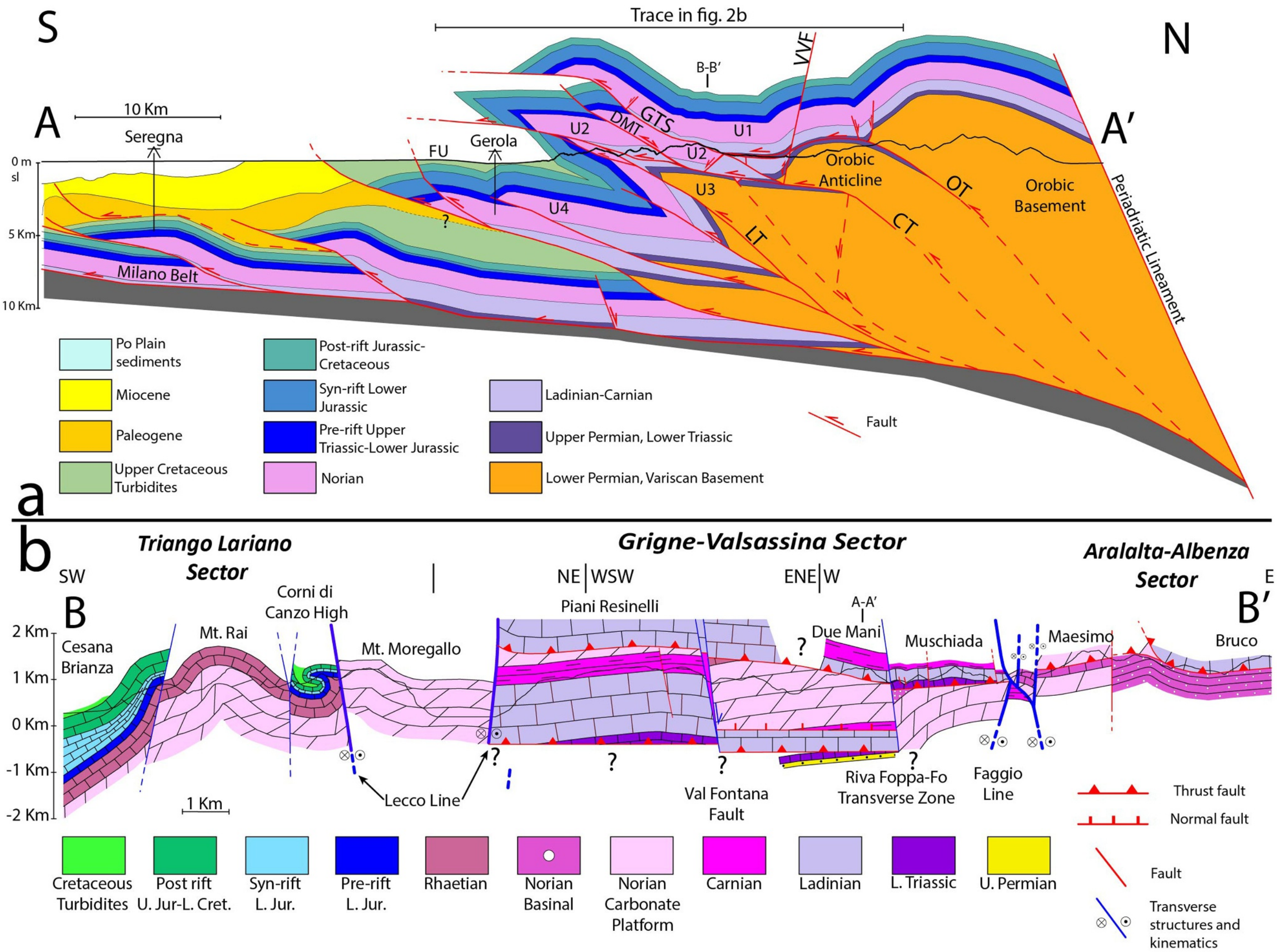

Figure 4. (a) N–S, balanced geological cross-section through the Central Southern Alps, from the Insubric Line to the Po-Plain, perpendicular to the main thrust faults. The southern part of the cross section was modified from Cassano et al. (1986), Pieri and Groppi (1981), Roeder (1992), and Schönborn (1992). OT: Orobic Thrust; GTS: Grigne Thrust System; CT: Coltignone Thrust; LT: Lecco Thrust: DMT: Due Mani Thrust; FU: Foothills Unit. Tectonic units are indicated with U1, U2, U3 (see Figure 2b). (b) SW-NE/W-E geological cross-section built perpendicularly to the main transverse zones of the study area.

dolostones and sabkha deposits (Servino Fm., Carniola di Bovegno; Cassinis, 1968), followed by Anisian shallow-water carbonates (Angolo Limestone; Assereto & Casati, 1965). During the Ladinian, thick carbonate platforms (Esino Lm.) were deposited above the Angolo Formation or the upper Anisian to lower Ladinian carbonate ramp and basin deposits (Prezzo Lms., Buchenstein Fm.; Berra et al., 2011, 2016; Gaetani et al., 1991). Coeval pelagic basins (Perledo-Varenna Fm.) developed heteropically with the Esino Lm. (Berra et al., 2011). During the Carnian, sedimentation occurred in mixed peritidal, lagoonal, and deltaic environments (Berra & Jadoul, 2002; Garzanti et al., 1995). A widespread carbonate platform formed in Norian time (Dolomia Principale Fm.), with the development of minor late Norian intraplatform basins, where clastic sedimentation occurred (Riva di Solto Shales; Jadoul et al., 1992). Carbonate platform growth resumed in Rhaetian–Early Jurassic time (Zu Lms., Albenza and Sedrina fms.). In Early Jurassic time, the platform drowned, and pelagic sedimentation occurred until the Early Cretaceous (Berra & Carminati, 2010; Bernoulli, 2007; Moltrasio Lms., Domaro Lms., Selcifero Lombardo, Maiolica Fm.). The Aptian–Albian marks the onset of foredeep sedimentation characterized by the deposition of turbiditic units such as the Bruntino Marls and the Sass de la Luna Fm. (Gaetani et al., 2012).

From top to bottom (from N to S), three major S-directed thrust sheets of Early Cretaceous-Cenozoic age are recognized in the Lecco area: Orobic Thrust (OT); Coltignone Thrust (CT); Lecco Thrust (LT; Figures 2a and 4a). They consist of successions characterized by considerable thickness and facies variations related to the following Mesozoic rifting stages, primarily associated with N–S striking normal faults (Berra & Carminati, 2010):

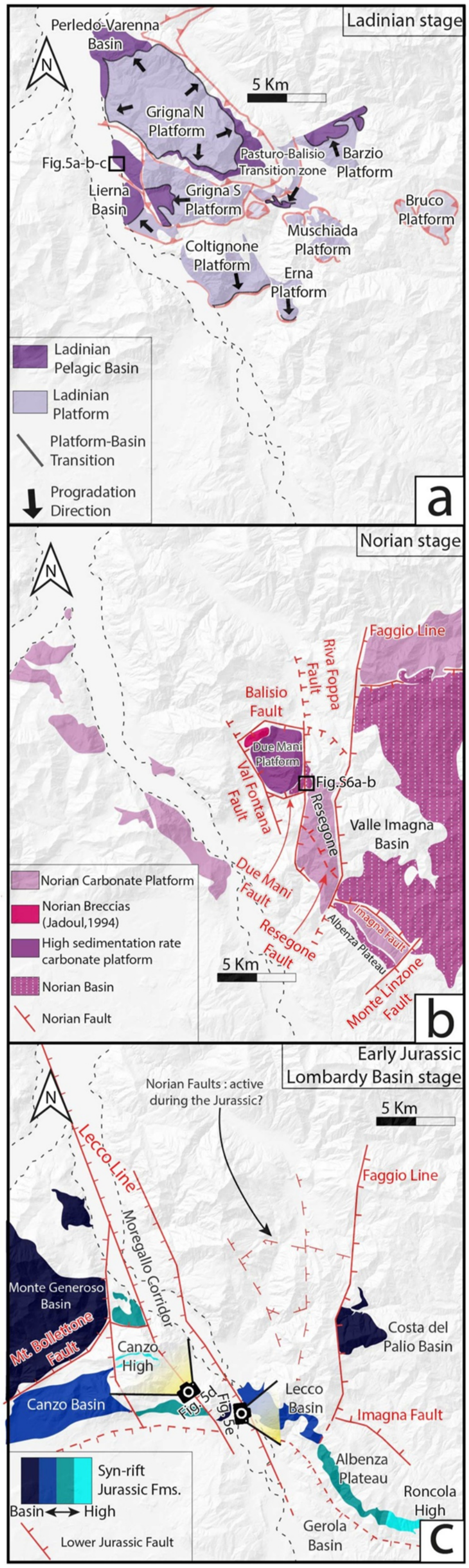

Figure 5. Paleogeographic maps for Mesozoic, pre-orogenic tectonic stages, with syn-tectonics rocks and faults highlighted. (a) Ladinian (with indicated present-day major thrusts). (b) Norian. (c) Early Jurassic.

- Late Norian, which led to the local development of fault-bounded, N–S elongated intraplatform basins with variable thicknesses within the Dolomia Principale Fm. (Berra & Jadoul, 1996; Jadoul et al., 1992).
- Early Jurassic, which produced N–S striking extensional faults and associated basins and led to the drowning of previous carbonate platforms (Bernoulli, 2007; Berra & Carminati, 2010; Rocca et al., 2024, 2026; Santantonio & Carminati, 2011).

The puzzling geometries of the thrust system observed in the area derive from the interference between these pre-orogenic structures and orogenic fault systems (Laubscher, 1985; Schönborn, 1992). Along-strike, the three major thrust sheets are subdivided into tectonic sub-units (Figure 2b), distinct on the basis of different stratigraphic settings, and are bounded by secondary and/or two major TZs (Lecco and Faggio Lines, Figures 2b, 3a, and 4b). These two faults were part of rift-related fault systems that controlled facies and thickness variations of Upper Triassic and Jurassic successions and the pre-orogenic lateral juxtaposition of rocks with different rheology (Schönborn, 1992). The Lecco Line is a NW–SE striking dextral fault zone mostly submerged by the Lecco Lake (de Sitter, 1960; Gianotti & Perotti, 1986; Jadoul & Gaetani, 1986; Laubscher, 1985; Schönborn, 1992). The Faggio Line is a N–S striking fault system (Jadoul & Gaetani, 1986; Schönborn, 1992) with strike-slip kinematics. However, the slip sense remains debated: according to Zanchi et al. (1988), this fault system exhibits complex kinematics with a dominant dextral component, whereas Schönborn (1992) described it as sinistral in the northern portion and dextral southward, as shown by the bending of the Flessura Pedemontana (FP) structure east of the Line (Figure 3a).

These two TZs bound the following tectonic sectors, each characterized by distinct shortening styles and different numbers of thrust faults (Figures 2 and 4b): (a) the Triangolo Lariano sector (west of the Lecco Line), where deformation is mainly accommodated by a series of E–W trending folds (Schönborn, 1992; Michetti et al., 2012; Figures 2a and 4b); (b) the Grigne-Valsassina sector (between the Lecco Line and the Faggio Line), characterized by a larger number of thrust faults (Laubscher, 1985; Schönborn, 1992); (c) the Aralalta-Albenza sector (east of the Faggio Line) that consists of a slightly deformed and folded plateau overlain by klippen. A detailed description of each sector is provided in TextS1 in Supporting Information S1.

The exposed front of the mountain belt is the "Flessura Pedemontana," a fault-related fold (Jadoul & Gaetani, 1986; Schönborn, 1992), which encompasses the three sectors and is strongly deflected across the Faggio Line (Figure 3a).

3. Methods

Field surveys, including original geological mapping, structural analysis, and sampling for U–Pb dating, were carried out along the main TZs, thrust faults and pre-orogenic structures. Fieldwork and the cartography presented here were based on published geological maps (Bersezio et al., 2014; Forcella et al., 2000; Gaetani et al., 2012; Jadoul, 1994; Michetti et al., 2012; Regione Lombardia, 2010; Schönborn, 1992). Structural data (attitudes of bedding, faults, lineations, foliation) were collected using Strabospot2 (Walker et al., 2019). A comprehensive geological map of the study area was produced using QGIS. A simplified version of the map is shown in Figure 3a, while a

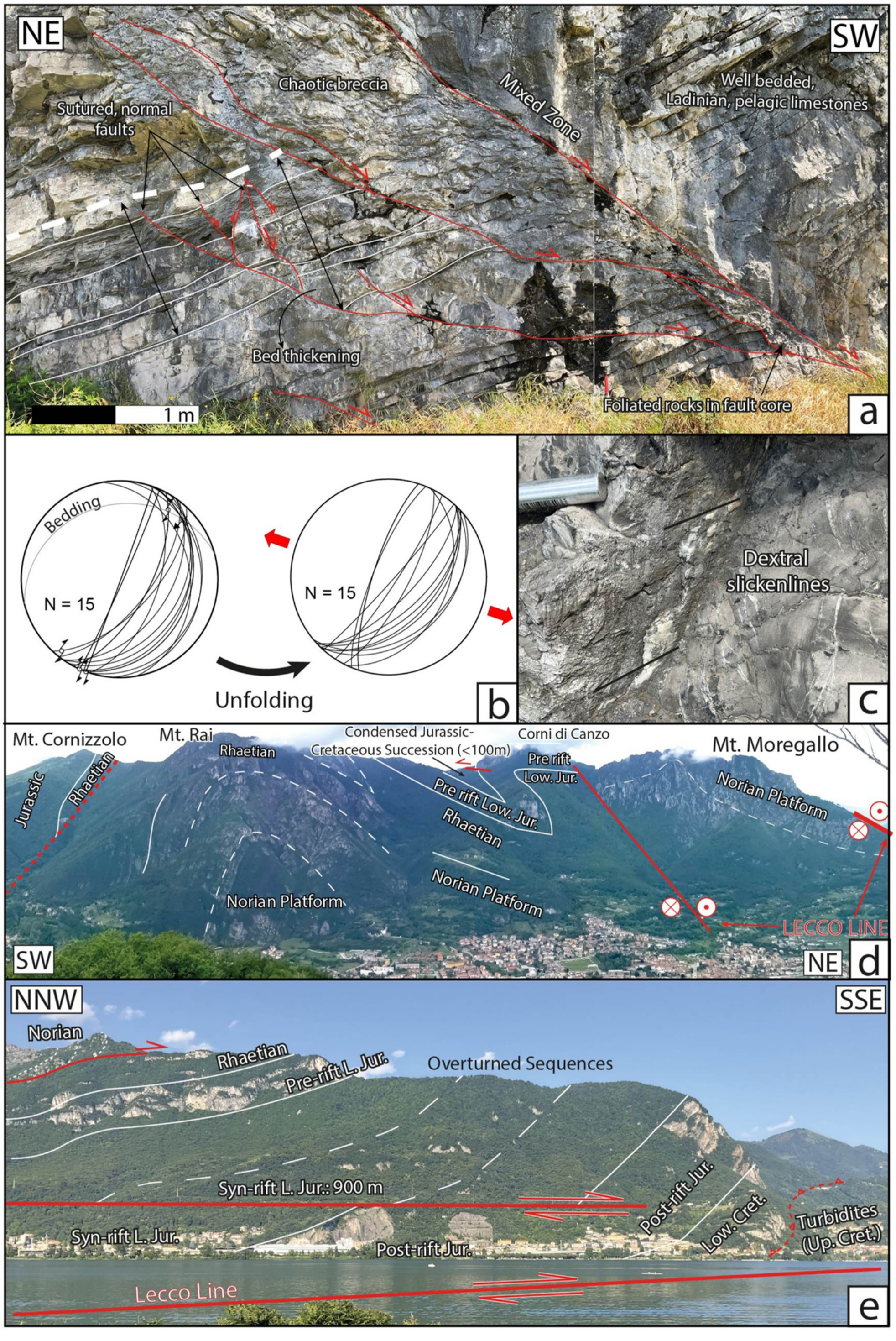

Figure 6. Mesozoic syn-sedimentary structures (locations in Figure 5) (a) syn-sedimentary normal faults within Ladinian basinal rocks; (b) Schmidt net (lower hemisphere) of the faults in (a), shown in present day orientation and after restoring the bedding to the horizontal; arrows show the inferred extension direction; (c) detail of dextral slickenfibers observed on a syn-sedimentary fault plane within Ladinian basinal rocks; (d, e) panoramic views showing the thickness contrasts of sediments between footwall (d) and hanging wall of the Lecco Line (e). Note the condensed succession of Jurassic-Cretaceous rocks (max 100 m) on top of the Corni di Canzo structural high in (d), today at the core of a tight syncline. On the eastern side of the Lecco Line, syn-rift, Lower Jurassic rocks are up to 900 m thick (e).

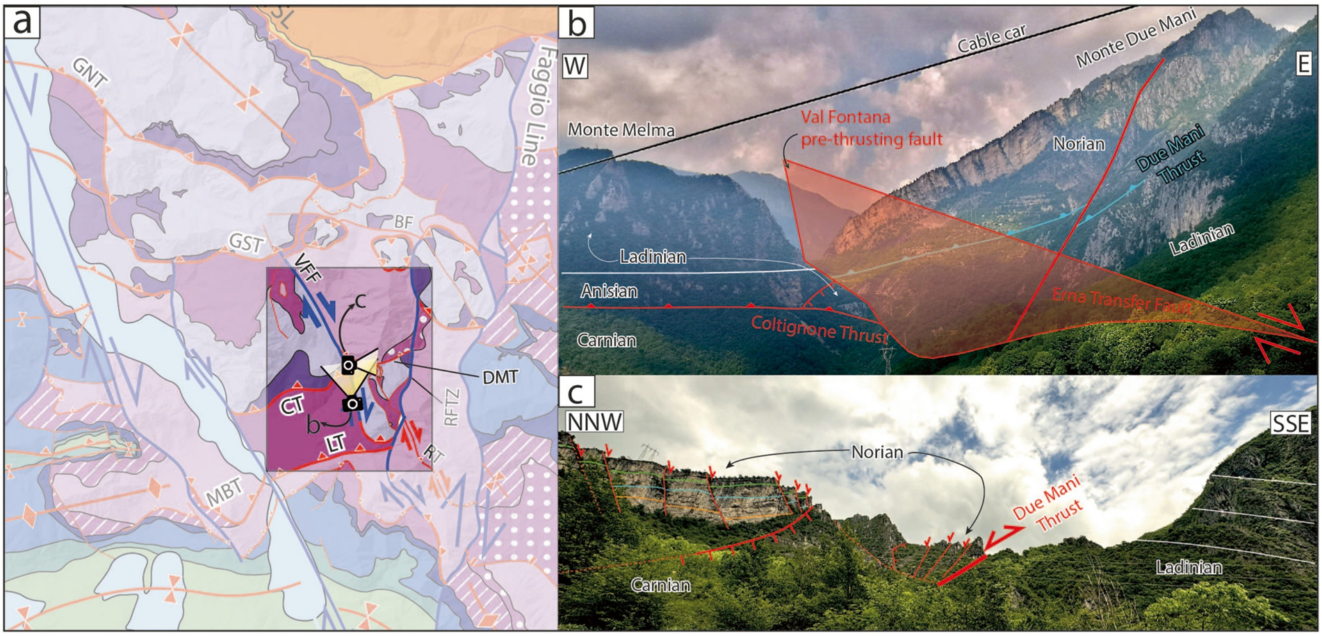

Figure 7. Alpine reactivation of pre-orogenic structures. In panel (a), the position of the panoramic views is indicated by stylized cameras. (b) The NW–SE striking pre-orogenic Val Fontana Fault was reactivated as a dextral transfer fault. (c) The Norian Due Mani fault was positively inverted during shortening, passively transporting a normal fault system in the hanging wall. Younger-on-older relationships are preserved.

more detailed version is provided in Figure S1 in Supporting Information S1. Stereographic projections were produced using Orient and WinTensor 5.9.2 (Delvaux & Sperner, 2003; Vollmer, 2015) on Schmidt nets, lower hemisphere. Fault planes and kinematic indicators were analyzed for paleostress reconstruction using Win-Tensor 5.9.2 (Delvaux & Sperner, 2003). Fault-slip data were first screened with the *P-T*-axes method to test the measured fault populations. The stress tensor was then obtained through the rotational optimization function, which iteratively minimizes the misfit between the data and the mean stress model to determine the stress-field orientation and the geometrical consistency among faults belonging to complex associations (Delvaux & Sperner, 2003). Geological cross-sections were constructed using MOVE software. A balanced geological cross section (down to the basal decollement) was drawn perpendicular to the main thrust faults (Figure 4a, A-A'), and inspired by previous interpretations (Cassano et al., 1986; Pieri & Groppi, 1981; Roeder, 1992; Schönborn, 1992). A shallower cross-section (Figure 4b, B-B') was constructed perpendicular to the main TZs of the study area (Lecco Line and Faggio Line).

Syn-tectonic carbonates (slickenfibres, veins, carbonate-cemented breccias) were collected from the fault zones after being photographed, structurally measured and associated with specific structures. Microstructural analysis was performed, using optical (Sapienza, University of Rome) and cathodoluminescence microscopy to identify different generations of carbonate phases, their habitus (blocky, elongated-blocky, etc.), growth mechanism, and crosscutting relationships. Cathodoluminescence (CL) analysis was carried out on polished thin sections at the Department of Earth Sciences of Sapienza University (Rome, Italy) and at the Department of Earth Sciences of ETH Zurich (Zurich, Switzerland). At Sapienza, CL analysis was carried out with a Leica DM2700P optical polarizing microscope equipped with a MK5 Optical, operating at a beam energy of 11 kV and beam current of 260 μA. At ETH, CL analysis was carried out with a Nikon Eclipse ME600 optical polarizing microscope equipped with a MK5, operating at a beam energy of 15 kV and beam current of 260 μA. In-situ U–Pb dating of each previously recognized carbonate phase was performed at the Department of Earth Science at the University of California, Santa Barbara, using an ESL ImageGeo 193 laser ablation system coupled to a Nu Instruments Plasma3D multicollector ICP-MS, following the analytical procedures by Kylander-Clark (2020). Of the 25 samples collected and analyzed, only 11 provided reliable ages. Further details on dating analytical techniques are provided in TextS2 in Supporting Information S1, while geochronological and structural data are shown in the EarthChem repository (Fiorini & Kylander-Clark, 2025).

During the preparation of this work, the author(s) used ChatGPT in order to improve readability and fluency. After using this tool/service, the author(s) reviewed and edited the content as needed and take(s) full responsibility for the content of the publication.

4. Results

In this section, we describe the pre-orogenic structures of the study area and their modes of reactivation as TZs during Alpine mountain building. We report observations made from regional to outcrop scales. Subsequently, we describe the microstructures of the sampled fault rocks and mineralizations and conclude with the results of the in situ U–Pb dating on carbonates. The results of geological mapping are reported in a detailed geological map (Figure S1 in Supporting Information S1). Figure 4a shows the geological cross-section A-A′, perpendicular to the main contractional structures, whose trace is shown in Figures 1b and 3a. Three main thrust systems are identified from north to south in Figure 4a: the OT, which includes the Grigne Thrust System (GTS) southward; the CT, characterized by several splays such as the Due Mani Thrust (DMT); the LT, part of the complex set of structures, which led to the polyphasic formation of the FP. Fault-bend folding is associated with the Orobic and the Coltignone Thrusts, while fault propagation folding characterizes the FP structure (Text S6 in Supporting Information S1). The frontal part of the belt consists of the thin-skinned Milano Belt, buried under the Po Plain sediments, and characterized by thrusts with flat-ramp-flat geometries (Roeder, 1992; Schönborn, 1992). The geological cross-section B-B' (Figure 4b, trace in Figure 3a) is drawn parallel to the main contractional structures. This section displays the difference in shortening style across the three tectonic sectors bounded by the Lecco and the Faggio Lines. In the western Triangolo Lariano Sector, deformation is accommodated by open to recumbent folds. In the central Grigne-Valsassina sector, shortening is accommodated by large displacement thrusts (Grigne Thrust and CT) interacting with second-order TZs (Val Fontana Fault and Riva Foppa-Fo TZ). The eastern Aralalta-Albenza sector is characterized by isolated klippen resting on the Norian successions.

4.1. Stratigraphic and Mesoscale Structural Analysis

4.1.1. Mesozoic Pre-Orogenic Tectonics

Significant lateral variations in stratigraphic thickness and facies, as well as extensional faults interpreted as pre-orogenic and rift-related, later reactivated as TZs, are shown in Figure 5 (further details in Text S4 in Supporting Information S1).

4.1.1.1. Middle Triassic

The highest mountains of the study area (Grigne, Coltignone, Erna, Muschiada) are composed predominantly of massive and thick Ladinian carbonate platform rocks (Esino Limestone; Figure 5a). Platform carbonates prograded onto coeval pelagic rocks (Perledo-Varenna Formation), exposed at lower elevations (eastern shore of Lake Como: Lierna, Perledo and Varenna areas; Valsassina: Pasturo-Balisio area, Figure 5a). Notably, the resulting heteropic contacts, corresponding to the platform margins, are parallel to major thrust faults (Figure 5a). Syn-depositional Triassic extensional faults are observed in basinal rocks near Lierna (Figure 6a). These SE-dipping tilted normal faults exhibit diagnostic growth fault features including bed thickening in the hanging wall, progressive increase of displacement in the dip direction and bed sealing of the faults (Figures 6a and 6b). Furthermore, the chaotic breccia constitutes the mixed zone of the main fault shown in Figure 6a, which developed under soft-sediment conditions (e.g., Caine & Minor, 2009). The syn-sedimentary structures are overprinted by brittle fault planes with dextral calcite slickenfibers (Figure 6c).

4.1.1.2. Late Norian

Upper Norian thin-bedded, dark dolostones (Dolomie Zonate Fm.) and black shales (Riva di Solto Shales) occasionally overlie massive carbonate-platform-related dolostones (Dolomia Principale Formation; Figure 5b, Figures S6a and S6b in Supporting Information S1). Significant lateral thickness variations indicate that their deposition was conditioned by major N–S (E-dipping) and minor E–W striking syn-depositional normal faults (Figure 5b). N–S faults, locally characterized by wedging of layers (e.g., Resegone Fault; Figure 5b and Figure S2b in Supporting Information S1), juxtapose carbonate platform successions with different thicknesses (likely reflecting different deposition rates; e.g., Val Fontana Fault) or different facies (e.g., Riva Foppa Fault; Figure 5b). The E-dipping Faggio Line marks the transition to the Valle Imagna Basin where the upper Norian

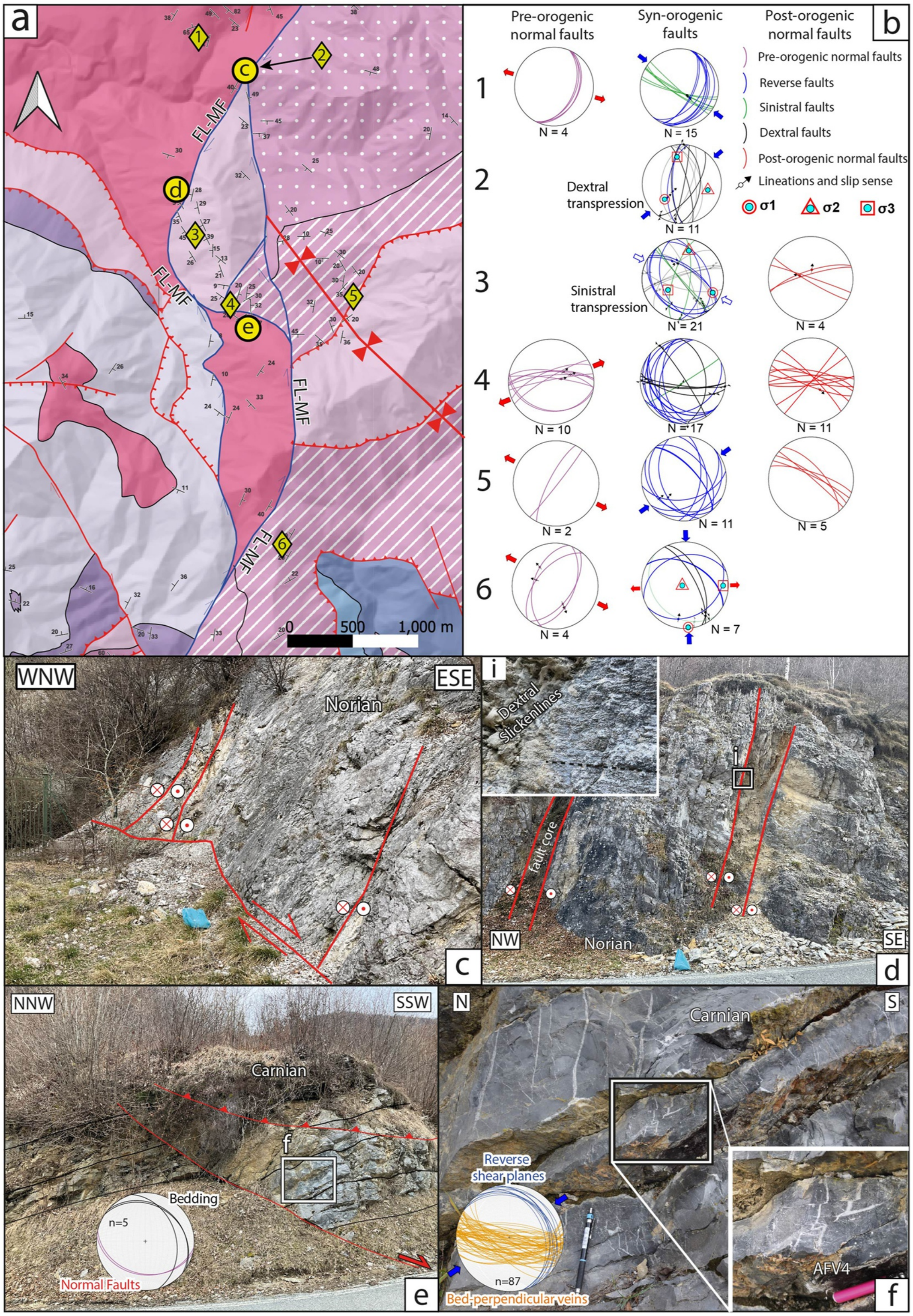
a
FL-MF
b
Pre-orogenic normal faults
Syn-orogenic faults
Post-orogenic normal faults
Pre-orogenic normal faults
Reverse faults
Sinistral faults
Dextral faults
Post-orogenic normal faults
Lineations and slip sense
σ1
σ2
σ3
Dextral transpression
Sinistral transpression
0 500 1,000 m
WNW
ESE
Norian
c
i
Dextral slickenlines
fault core
NW
SE
d
NNW
SSW
Carnian
Bedding
n=5
Normal Faults
e
N
S
Reverse shear planes
n=87
Bed-perpendicular veins
AFV4
f

Figure 8.

basinal rocks reach their maximum thickness (Figure 5b). In this area, the Norian carbonate platform rocks are <1,000 m thick, whereas basinal formations reach maximum thicknesses of 500–600 m. The geometry and distribution of these depocenters are also controlled by minor E–W oriented faults that bound these depressions (Figure 5b). The E–W Due Mani Fault zone locally displays Norian basinal rocks in the hanging wall and preserves younger-on-older relationships. As detailed below, the Due Mani Fault and several associated minor E–W and N–S striking extensional structures were reactivated during the Alpine orogeny (see Sections 4.1.2 and 5.2).

4.1.1.3. Early Jurassic

The Early Jurassic structural architecture was mainly dominated by N–S striking normal faults (Figure 5c). The largest Early Jurassic pelagic basin of the study area is the Monte Generoso Basin, which formed in the hanging wall of the extensional, E-dipping listric Lugano Fault (Bertotti, 1991), located ∼20 km to the west of the area shown in Figure 5c. This pelagic basin reaches a thickness exceeding 2,000 m at its depocenter (Michetti et al., 2012). Toward the east, and partly to the south, the syn-rift deposits thin significantly, becoming less than 50 m at the structural culmination of the Canzo High (Figures 5c and 6d). Minor W/NW-dipping normal faults (e.g., Monte Bollettone Fault, Figure 5c) antithetic to the Lugano Fault partially control these thickness variations. A significant increase in syn-rift sediment thickness (up to 900 m) is observed toward the eastern shore of Lake Como (Figure 6e). This thickening coincides with the present-day trace of the NW–SE striking, E-dipping western branch of the Lecco Line (Figure 5c). A W-dipping fault, conjugate to this master fault, morphologically follows the southern branch of Lake Como and emerges northward as a vertical fault (Figures 2, 3a, and 5c). Evidence for the occurrence of this antithetic fault is further discussed in Text S4 in Supporting Information S1.

Farther east, the Early to Middle Jurassic reactivation of the E-dipping Faggio Line led to the development of a basin (Costa del Palio Basin; Jadoul & Doniselli, 1986; Schönborn, 1992; Figure 5c). The presence of tilted low-angle normal faults crosscut by contractional structures supports a pre-orogenic phase of activity along the Faggio Line (Figures 8e and 8f; further details in Section 4.1.2). To the south, the Imagna Fault was likely active during the Early Jurassic, as evidenced by the reduced thickness of the syn-rift formations in the eastern part of the Albenza Plateau with respect to the Costa del Palio Basin (Figure 5c, Roncola High, Bersezio et al., 2014). South of the Imagna Fault, syn-rift deposits of the Lecco Basin (∼900 m thick) progressively thin out eastwards across the Albenza Plateau (ranging from 700 to 100 m, west to east; Figure 5c). Farther south, syn-rift formations buried beneath the Cretaceous turbidites are encountered in the Gerola well (Figure 4a). They are as thick (∼900 m) as those of the Lecco Basin, and thicker than those in the Albenza plateau and farther east. This suggests the presence of a S/SW-dipping fault separating the Albenza plateau from the Gerola Basin (Figure 5c), likely located beneath the present-day position of the FP structure in the Aralalta-Albenza sector.

4.1.2. Mesozoic-Cenozoic Shortening

Most of the Mesozoic extensional faults were oriented N–S and NW–SE, either parallel or oblique to the predominant N–S directed Alpine compression (Figure 5). During orogenic shortening, many of these faults were likely reactivated as transfer faults and/or lateral ramps (Figure 7b). Concerning E–W Mesozoic faults, those dipping to the south were commonly beheaded and passively transported along contractional structures. In contrast, N-dipping normal faults frequently display evidence of incomplete positive inversion, preserving the younger-on-older relationships typical of normal faulting (Figure 7c).

Figure 8. Structural analysis of the Faggio Line in Culmine S. Pietro area. (a) Geological Map of Culmine S. Pietro area. FL-MF: Faggio Line-Main Fault. Legend is the same of Figure 3b. The location of the outcrops of panels (c–f) is shown with circles. Location of structural stations in panel (b) is shown with diamonds. (b) Stereonets (Schmidt net, lower hemisphere) of the faults outcropping in the Culmine S. Pietro. Numbers on the left refer to the structural stations indicated in (a). Arrows show the inferred compression(blue)/extension(red) direction from fault/slip data. At stations 2, 3, and 6 fault–slip inversion and paleostress reconstructions were performed on the highlighted syn-orogenic fault planes; poorly fitting/inconsistent planes are blurred. Solutions were accepted for average values of the F5 rotational optimization function below 30, based on previous experiences (Delvaux & Sperner, 2003; Rocca et al., 2026). More details are shown in Figures S4e–S4h in Supporting Information S1. (c) Principal fault plane of the Faggio Line, with dextral Riedel R faults; (d) Sub-vertical fault planes close to the main fault within Norian dolostones, showing dextral slickenlines. (e) S-dipping, low-angle normal faults and N–S reverse faults cropping out along the E–W undulation of the main fault. (f) Site of sample AFV4, analyzed for U–Pb absolute dating. E–W striking, subvertical calcite veins are displaced by small ENE-dipping reverse shear planes filled by calcite. Arrows show the compression direction inferred from fault geometry and kinematics.

In the following, we focus our meso-structural observations on the two principal N–S TZs—the Faggio and the Lecco lines—and on the E–W DMT, a positively inverted normal fault. A detailed description of the Riva Foppa-Fo TZ and the Resegone Thrust (RT) is provided in Text S3, Figures S2, and S3 in Supporting Information S1.

4.1.2.1. Faggio Line

The Faggio Line is exposed discontinuously (Figures 2b and 3a). Our structural analysis focuses on the Culmine San Pietro area (Figure 8a, location in Figure 3a), where the TZ crops out as a broad deformation zone. The fault zone mainly strikes N–S/NNE-SSW (Figures 2b, 3a, and 8a), but a significant change in orientation occurs in the central portion of the study area, where it strikes WNW–ESE, before re-attaining its main N–S/NNE-SSW trend southward (Figure 8a). We identified pre- and post-orogenic normal faults, based on cross-cutting relationships with contractional structures (strike-slip and reverse faults; Figure 8b). Pre-orogenic normal faults follow the overall trend of the Faggio Line (i.e., N–S/NNE–SSW in structural stations 1, 5 and 6; E–W in structural station 4; Figure 8b). Their kinematic indicators point to an overall E–W oriented extension in pre-orogenic times. Relationships between pre- and syn-orogenic structures are observable south of structural station 4, where E-dipping reverse faults displace low-angle E–W striking tilted normal faults (Figures 8e and 8f) occurring in Carnian rocks (Gorno Fm.). Furthermore, E–W bed-perpendicular veins parallel to and associated with these normal faults are crosscut by ENE-dipping reverse shear planes decorated by calcite mineralizations, with an orientation similar to the overall N–S strike of the Faggio Line (Figure 8f).

Strike-slip and reverse orogenic faults show more chaotic orientations (Figure 8b) and are characterized by unclear cross-cutting relationships, usually mutual. Structures measured along and close to the main fault display dextral strike-slip kinematics consistent with parallel or R-type faults (Figures 8c and 8d, Figure S4i in Supporting Information S1). They are more organized in structural stations 2 and 6, where they strike mostly N–S and NNW–SSE, respectively (Figure 8b). In some cases, the main faults cut a steep foliation occurring in marly rocks (Carnian?; Figure S4i in Supporting Information S1). Inversion of fault planes and kinematic indicators for structural stations 2 and 6 indicate NE-SW and N–S orientations of the maximum horizontal stress, respectively (Figure 8b, Figures S4e and S4g in Supporting Information S1). This state of stress is consistent with ca. NW–SE striking transpressional faults and shear planes and observed NE-directed vergence (Figure 8b, structural stations n. 3–6), and with the top-to-S movement of the ENE-dipping reverse shear planes in Figure 8f. Furthermore, east of the Faggio Line the thrust surface of the Maesimo Klippe, where Norian dolostones overthrust Rhaetian limestones and marls (Figure 8a), is folded as a synform with a NW–SE hinge, consistent with outcrop-scale folds in the footwall, associated with NW–SE striking reverse faults (Figures 8a and 8b, structural station n.5; S4b in Supporting Information S1). Similar NW–SE fold hinges east of the Faggio Line have also been observed to the south, in Rhaetian Limestones (Gaetani et al., 2012; Figure S4k in Supporting Information S1). At stations 3–4 the structural assemblage is more complex. NW–SE and E–W striking faults occur consistently with the progressive bending of the Line (Figure 8b). Moreover, dextral and sinistral strike-slip faults coexist (Figure 8b). In structural station 3 (Figure 8b), N–S and NW–SE striking sinistral faults and NW–SE striking, SE-verging transpressional faults were observed. Inversion of fault planes and kinematic indicators from these stations suggests a NW–SE oriented maximum horizontal stress (Figure 8b, Figure S4f in Supporting Information S1). This state of stress is also consistent with the occurrence of several E–W striking, antithetic dextral faults (Figure 8b). NW–SE striking sinistral faults were also observed in structural station 1 (Figure 8b), associated with SE-dipping reverse faults (Figure 8b). South of the Culmine S. Pietro area, east of the Faggio Line, structural complexity is illustrated by a set of SW-dipping reverse faults and E–W striking sinistral faults in Lower Jurassic, syn-rift limestones (Figure S4j in Supporting Information S1). Post-orogenic, mainly WNW–ESE striking normal faults displace these contractional structures (Figure 8b). Southward, the structural complexity decreases, and the Faggio Line crops out as a discrete dextral strike-slip fault plane (e.g., at Pertus Pass; Supporting Information, Text S5, Figure S4 in Supporting Information S1), associated with NE-SW striking dextral mesoscale faults and maximum paleostress axis (Figure S4h in Supporting Information S1).

4.1.2.2. Lecco Line

The structural analyses along the NW–SE striking Lecco Line were made at two key localities along the western shore of Lake Lecco, between the two branches of the fault (Figure 9a). In an abandoned quarry in the northern portion of the Moregallo unit (U3, Figures 2b and 9b–9d), Norian carbonate platform dolostones, exposed immediately east of the TZ, display pervasive minor faulting, cataclasis, brecciation and fracturing (Figures 9c

10.1029/2025TC009200

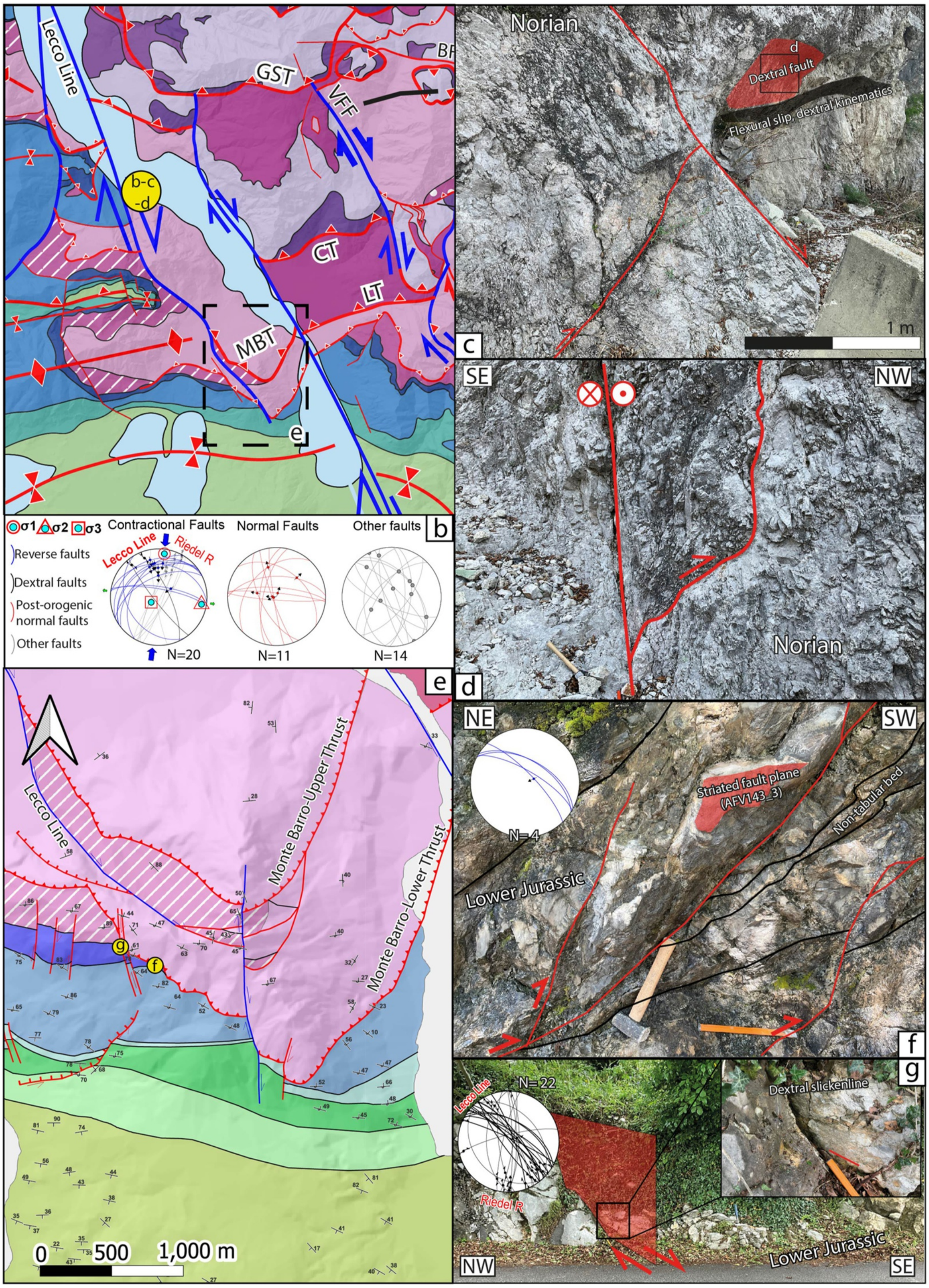

Figure 9. Lecco Line structural analysis. (a) Geological map showing the location of the outcrops of panels (b–d) and of the close-up map of panel (e). Legend is the same of Figure 3b. (b) Stereonets (Schmidt net, lower hemisphere) of the faults cropping out in the abandoned quarry (Locality: Moregge). Fault–slip inversion and paleostress reconstructions were performed on the highlighted contractional faults; poorly fitting/inconsistent planes are blurred. More details are shown in Figure S5d in Supporting Information S1. (c) Interaction between strike-slip, reverse and normal faults. Normal faults displace the others. (d) Positive flower structure forming from a dextral fault. (d) Geological map of the Monte Barro area, showing the location of the outcrops of panels (f) and (g). (e) Geological map of the Monte Barro area. Legend is the same of Figure 3b. (f) Reverse fault planes immediately south the Monte Barro Lower Thrust, decorated with slickenfibers (sampled for U–Pb absolute dating, sample AFV143_3) within Lower Jurassic, non-tabular beds. Orientation of the reverse fault is plotted in the stereonet (Schmidt net, lower hemisphere). (g) Subvertical dextral transfer faults (as suggested by slickenlines) displacing the Monte Barro lower thrust. Orientation of the dextral faults is plotted in the stereonet (Schmidt net, lower hemisphere).

and 9d). Dextral faults mainly strike NNE-SSW and are associated with NNW–SSE striking faults (Figure 9b). The NNE–SSW striking faults are likely R-type dextral faults of the NNW–SSE oriented TZ, which is parallel to the second set. NNW-dipping, top-to-S, reverse faults are also associated with strike-slip faults, forming positive flower structures (Figures 9b and 9d). Bedding planes typically exhibit dextral shearing (Figure 9c). Our paleostress reconstruction suggests a NNE–SSW oriented maximum stress axis, consistent with a dextral reactivation of the Lecco Line (Figure 9b, Figure S5d in Supporting Information S1). Normal faults with chaotic orientations and slip directions (Figure 9b) cut across these reverse and strike-slip structures (Figure 9c).

Further south, the Lecco Line intersects the structures of the FP in the Monte Barro area, where Norian platform carbonates structurally overlie overturned, N-dipping Rhaetian to Cretaceous rocks along two N-dipping thrust surfaces (Figures 2, 3a, and 9e; S5a in Supporting Information S1). These thrusts are situated between the two branches of the Lecco Line. The upper thrust terminates at the western branch, whereas the lower thrust is offset by dextral NW–SE striking transfer faults, parallel to the Lecco Line (Figure 9e). Between these thrust surfaces, bedding planes in the Norian and Rhaetian rocks strike E–W ranging from upright to overturned (Figure 9e). Immediately beneath the lower thrust surface, NNE-dipping reverse faults occur within Lower Jurassic, syn- and pre-rifting carbonates (Figure 9f). Reverse faults are steep (up to 70°) and decorated with slickenfibers. Parasitic folds bounded by reverse faults in the footwall of the Monte Barro Thrust (MBT) system are consistent with SSW-directed vergence (Figure S5b in Supporting Information S1). Several N–S and NW–SE striking dextral strike-slip faults were recognized throughout the area (Figure 9g), with orientations consistent with that of the Lecco Line. At the map scale, major dextral faults act as transfer faults of thrusts (Figure 9e). At the outcrop scale, the MBT and the Lecco Line-related minor structures (joints, sheared veins, horizontal and subvertical veins, minor faults) display mutual crosscutting relationships (Figure S5c in Supporting Information S1).

4.1.2.3. Due Mani Thrust

The DMT is a hanging wall splay of the CT, part of thrust sheet 2 (Figures 2 and 4a). The thrust is bounded by two secondary TZs, the Val Fontana Fault to the west and the Riva Foppa-Fo TZ to the east (Figure 10a). This N-dipping thrust fault is characterized by younger-on-older relationships. The hanging wall is composed of Norian dolostones, and the footwall of Ladinian carbonate-platform successions (Figure 10a). The fault core comprises a meter-scale zone of foliated polychrome Carnian pelites, bounded by distinct fault planes at the contacts with Norian and Ladinian rocks (Figure 10b; Figures S6c, S6e, and S6f in Supporting Information S1). Both the hanging wall and footwall are dissected by N–S and E–W normal faults, crosscut by the main thrust fault zone (Figures 10a and 10f; Figures S6a and S6b in Supporting Information S1). The main thrust is exposed at several localities along the road from Ballabio to Morterone (Figure 10b; Figures S6c, S6e, and S6f in Supporting Information S1), and dips to the NW with dip angles generally decreasing eastward. S-C-like foliations within Carnian marls hosting the fault core indicate a SE-directed sense of shear (Figure 10b; Figures S6c and S6d in Supporting Information S1; Schönborn, 1992), consistent with a NW–SE oriented shortening. Locally, blocks of Ladinian limestones are embedded within the foliated Carnian pelites; E–W striking normal faults form the contacts between these two as R′ antithetic faults of the thrust (Figure 10b). In the hanging wall, N–S fault planes, oblique to perpendicular to the main thrust surface, are observed, mostly dipping eastward (Figure 10c). These fault zones exhibit intense cataclasis, S–C-type fabrics, sigmoidal lithons, and striated fault surfaces, consistent with a NW–SE shortening (Figure 10c). In some cases, kinematic indicators point to strike-slip movements. In the easternmost sector of the area, hanging wall Norian dolostones pass to basinal shales, with the primary boundary defined by the N–S striking, Riva Foppa-Fo TZ (Figure 5c; S6a, S6b; S10a, and S10d in Supporting Information S1). Here, E–W striking (Figure 10d) tilted normal faults occur, displaying evidence of positive inversion, including striations, folds and displacement (Figures 10d and 10e). Slickenlines reveal a significant lateral slip component along these faults. Locally, fault core foliation is crosscut and dragged by N–S striking transtensional faults, as constrained by S-C–C′ structures, which point to an extensional overprint, postdating shortening (Figures S6g and S6h in Supporting Information S1).

4.2. Microstructural Analysis and U–Pb Carbonate Dating

The syn-tectonic carbonate samples collected for U–Pb dating include slickenfibers on fault planes or bedding surfaces (flexural slip), veins along S-C thrust-related foliation, bed-parallel and bed-perpendicular veins, veins parallel to or precipitated along the main faults, and carbonate-cemented breccias. Microstructural observations generally support previous observations of multiple diachronous tectonic events along the thrust faults and,

10.1029/2025TC009200

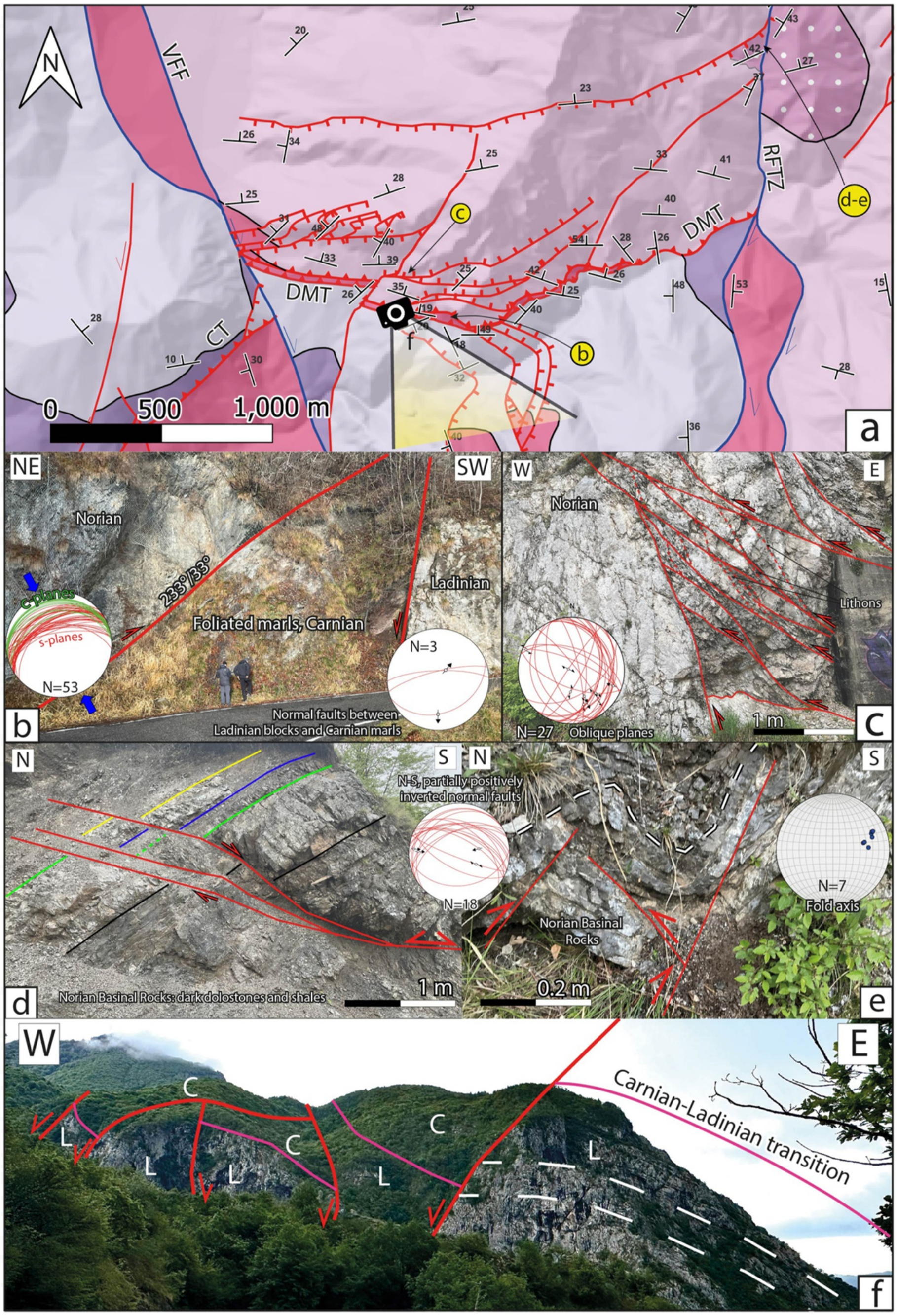

Figure 10. (a) Geological map of the Due Mani Thrust (DMT) area, legend is the same of Figure 3b. The location of the outcrops of panels (b–e) is shown. The position of the panoramic view is indicated by the stylized camera. VFF: Val Fontana Fault, CT: Coltignone Thrust, DMT: Due Mani Thrust; RFTZ: Riva Foppa-Fo Transverse Zone. (b) DMT juxtaposing Norian rocks at the hanginwall and Carnian rocks at the footwall, where the fault core developed. S-C foliation in the Carnian rocks indicates SE-directed vergence, as indicated by arrows. Locally in the fault core, block of Ladinian platform rocks occur. Contacts between these blocks and the Carnian units are normal faults. (c) N–S striking oblique fault planes showing S-C like structures and lithons, indicating WNW-directed vergence. (d) E–W oriented normal faults. Extensional displacement of different lithologies is observed. Normal faults exhibit inversion structures, as suggested by associated folds (e) with axis orientation consistent with the vergence of the DMT. (f) Panoramic view showing normal faults in the footwall of DMT, composed of Ladinian limestones, displacing the Carnian-Ladinian boundary. Representes stereonets are Schmidt net, lower hemisphere projections.

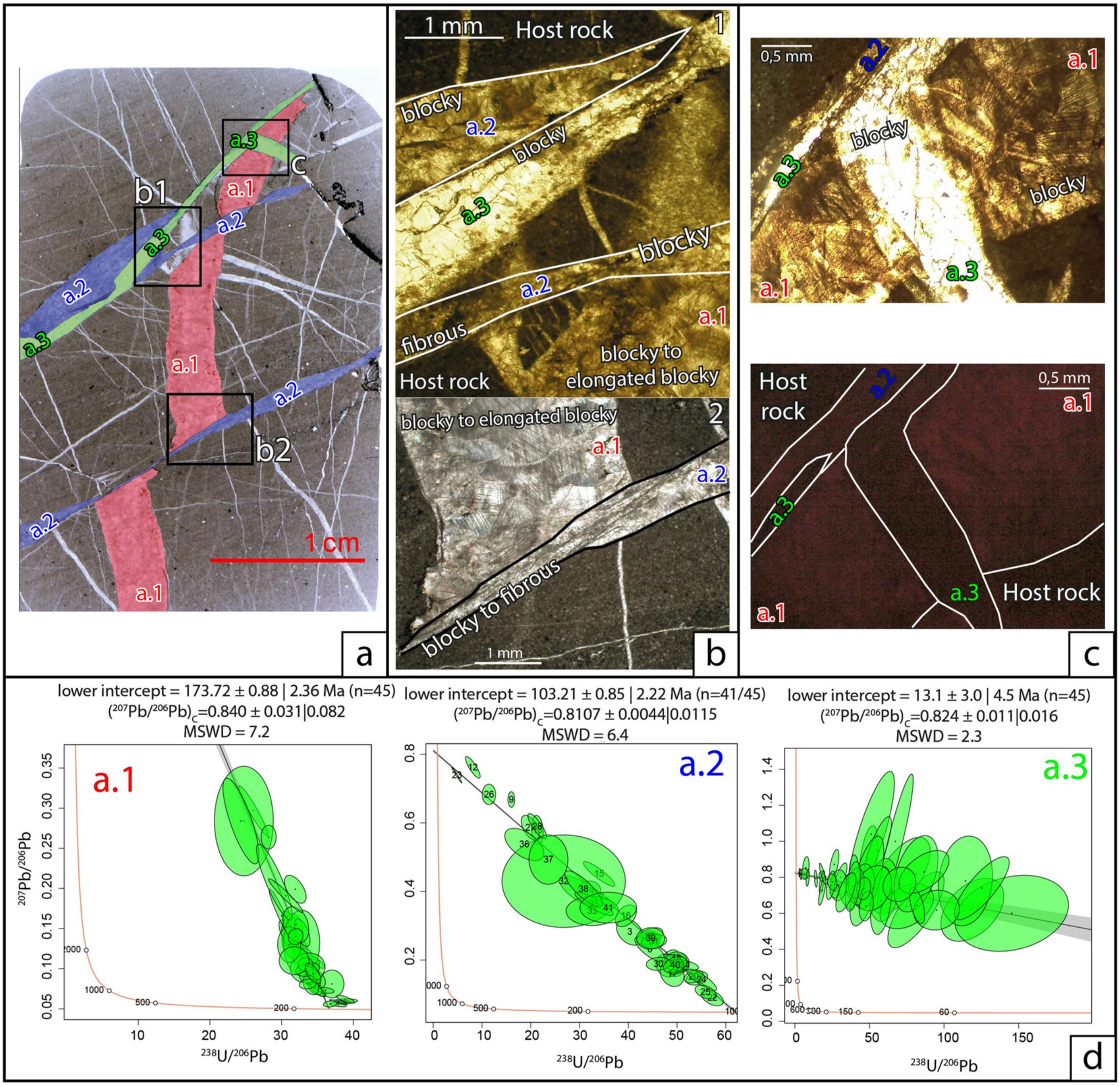

Figure 11. Microstructural analysis of sample AFV4, collected within the Faggio Line fault zone (see Figures 8e and 8f). (a) Whole-section image, showing the three sets of veins that were analyzed. In chronological order: red (a.1), bed-perpendicular, E–W striking calcite vein related to a normal fault system; blue (a.2), calcite decorating ENE-dipping reverse shear planes cutting (a.1); green (a.3), vein precipitated after reopening of (a.2). (b) Cross cutting relationship and textures of the (a.1–a.3) veins. (c) Cathodoluminescence microscopy images. a.1 and a.2 show very dull cathodoluminescence as the host rock. a.3 is completely not cathodoluminescent. (d) Tera-Wasserburg graphs showing the results of the U–Pb absolute dating analyses performed on the (a.1–a.3) veins.

particularly, the TZs of the study area. Among these, we have: clear cross-cutting relationships (Figure 11; Figures S7, S8, S10, S13, S14, S15 in Supporting Information S1); crack-and-seal events (Figures S10 and S12 in Supporting Information S1); slickenfibers with several superimposed sheets (Figures S7, S9, and S14 in Supporting Information S1); texture or cathodoluminescence changes among different sheets, sealing events, veins (Figure 11; Figures S7, S8, S10, S11, and S14 in Supporting Information S1). Similar microstructural evidence of multiple reactivations of faults has been observed in other works (e.g., Becker et al., 2011; Bilau et al., 2023; Luo et al., 2020; Parizot et al., 2022; Smeraglia et al., 2018; Tillberg et al., 2020). A description of each thin section

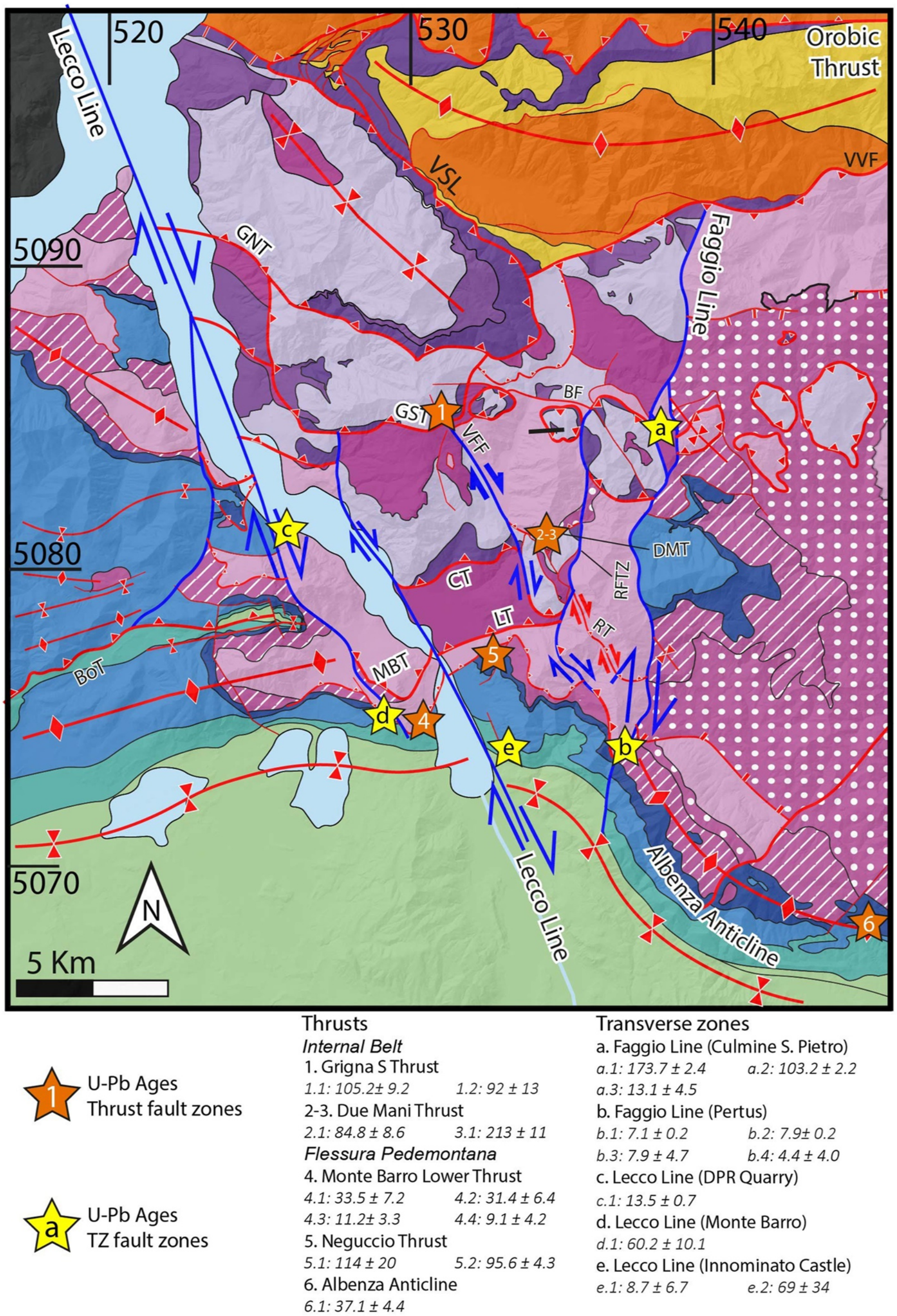

Figure 12. Geological map of the study area showing the sampling localities and the absolute dating obtained after U–Pb analysis on syn-tectonic carbonates. Legend is the same of Figure 3b. Syn-tectonic mineralizations were distinguished for samples collected within thrust fault zones and transverse zones.

that yielded interpretable ages ($n = 11$) is provided in the following paragraphs. In these descriptions, dated carbonate phases are labeled using a two-part code in a X.Y format, where X identifies the thin section and Y identifies the specific analyzed carbonate phase within it. Thin sections collected along present-day TZs are denoted by a letter in the first position (letter.number), whereas thin sections collected along thrusts are denoted by a numeric identifier in the first position (number.number). Sample locations and corresponding ages are presented in Figure 12. Table 1 summarizes the features of the dated carbonates. Data from U–Pb analyses are available at EarthChem repository (Fiorini & Kylander-Clark, 2025) under CC-BY-4.0. Tera-Wasserburg plots are shown in Figure 11 and in Figures S7–S16 in Supporting Information S1. Ages are reported with propagated 2σ systematic uncertainty. Some samples display high errors due to low $^{238}U/^{206}Pb$ values, initial lead uncertainties, high MSWD, or (partly) overlapping, close-in-age carbonate generations. Even though they cannot always provide precise information on the tectonic evolution of the area, these data are included because they can still provide constraints on the longevity of TZs and thrusts. Slickenfibers developed along fault planes are interpreted as associated with fault slip (Roberts & Holdsworth, 2022). Therefore, they provide the most direct constraints on fault-slip timing when the microstructural link to slip is clear. In contrast, veins in fault damage zones and breccia cements may also form due to later fluid circulation and fracture sealing processes within fault zones (Renard et al., 2000). Consequently, they constrain the timing of the broader deformation context in which damage zones developed and evolved, rather than discrete slip events (Roberts & Holdsworth, 2022; Virgo et al., 2014). Samples characterized by multiple generations of carbonate phases yield different ages, systematically younger than the host-rock stratigraphic age, even when 2σ errors are considered. Furthermore, these multiple ages show that syn-tectonic carbonates keep their original U–Pb age even after later reactivation, which supports the use of calcite U–Pb dating to track long-term fault activity (see also Parizot et al., 2022).

4.2.1. Transverse Zones—Faggio Line

Sample AFV4 (Figure 11), collected along the Faggio Line TZ in the Culmine di San Pietro area (Figures 8e, 8f, 11, and 12, see Section 4.1.1), exemplifies a polyphase structure observed in this sector of the CSA. The earliest structures consist of bed-perpendicular, E–W striking veins (a.1), interpreted as deposited in extensional fractures associated with a normal fault system (Figures 8e, 8f, 11a, and 11b). These are clearly crosscut by ENE-dipping reverse shear planes (a.2), striking parallel to the Faggio Line, indicative of a subsequent compressional phase (Figures 8f, 11a, and 11b). A younger carbonate generation (a.3) precipitated during later local reopening of the contractional structures. The earliest vein generation (a.1) is composed of blocky to elongated-blocky calcite, which is dull red under CL and only slightly distinguishable from the host rock (Figure 11c). The second vein generation (a.2), associated with reverse shear planes, consists of blocky to fibrous calcite and is similarly dull red under CL (Figure 11c). The youngest vein generation (a.3) is characterized by blocky calcite that is non-luminescent under CL (Figure 11c). a.1 yielded an age of 173.7 ± 2.4 Ma; a.2 yielded an age of 103.2 ± 2.2 Ma; a.3 yielded an age of 13.1 ± 4.5 Ma, constraining the timing of multiple episodes of fracture (re)opening and sealing within the fault zone.

Sample AFV105 (Figure S7 in Supporting Information S1) was collected forelandward along the line in Rhaetian Limestones of the FP structure, at Pertus Pass (Figure S4 in Supporting Information S1; Figure 12). It consists of calcite slickenfibers on a Riedel R dextral fault plane associated with the main Faggio Line. Three layers (b.1 to b.3) are superimposed along the same surface, crosscutting earlier tooth-shaped veins (b.4) oriented at a high angle. The three slickenfiber layers consist of blocky calcite, with crystal sizes ranging from tens of microns to several millimeters, and the lowest sheet (b.3) appears brecciated. Under CL, b.1, b.2 and b.3 are dull to non-luminescent. b.4 consists of fibrous calcite and is completely non-luminescent. b.1 yielded an age of 7.1 ± 0.2 Ma, b.2 an age of 7.9 ± 0.2 Ma, b.3 an age of 7.9 ± 4.7 Ma. These are indicative of fault-related slip. b.4 yielded an age of 4.4 ± 4.0 Ma, constraining the timing of sealing of tooth-shaped fractures.

4.2.2. Transverse Zones—Lecco Line

Sample AFV60 (Figure S8 in Supporting Information S1) was collected at the abandoned Moregallo quarry site (Figures 9a–9c and 12) within Norian dolostones of thrust sheet 3 (Figure 2a). It consists of sheared veins on a dextral fault plane within the Lecco Line fault zone, crosscutting bed-perpendicular veins at 80° (c.1). The thin section shows that sheared veins are composed of saddle dolomite, which forms cm-scale crystals. Bed-perpendicular veins are composed of dolomite, with uncertain habit due to their small size. Under CL, saddle dolomite is dull, while bed-perpendicular veins are non-luminescent. The saddle dolomite phase did not yield interpretable ages. Bed-perpendicular veins (c.1) yielded an age of 13.5 ± 0.7 Ma, constraining the timing of an early fracture-opening and sealing event. These veins are crosscut by sheared veins developed along the dextral fault plane, providing a post-veining indirect constraint for the timing of fault slip.

Sample AFV144 (Figure S9 in Supporting Information S1) is a dextral slickenfiber decorating a fault plane related to the Lecco Line interfering with the MBT system, part of the FP structure (Figure 12). The sample comes from Lower Jurassic, syn-rift limestones at the footwall of the thrust system. The slickenfiber is composed of

Table 1
Features of the Dated Carbonates

Sample name	Fault zone	Host rock	Tectonic unit	Latitude	Longitude	Cement s	Mineral	Structures	Habitus	Age (Ma)
Transverse zones-related dated carbonates										
AFV4	Faggio Line	Carnian Units (Fm. Gorno)	Barzio Unit (U2)	45.9132	9.4949	a.1	Calcite	High angle vein related to normal faults	Blocky to elongated blocky	173.7 ± 2.4
						a.2	Calcite	Mineralizations filling reverse shear planes cutting a.1	Fibrous to blocky	103.2 ± 2.2
						a.3	Calcite	Mineralizations precipitated after reopening of a.2	Blocky	13.1 ± 4.5
AFV105	Faggio Line (Pertus)	Rhaetian (Zu Lms.)	Albenza Unit, Flessura Pedemontana (UII.I)	45.8185	9.4772	b.1	Calcite	Dextral slickenfiber, upper sheet	Blocky	7.1 ± 0.2
						b.2	Calcite	Dextral slickenfiber, intermediate sheet	Blocky (microcristalline)	7.9 ± 0.2
						b.3	Calcite	Dextral slickenfiber, lower sheet. Brecciated portion.	Blocky	7.9 ± 4.7
						b.4	Calcite	Tooth-shaped vein, cut by slickenfiber	Fibrous	4.4 ± 4.0
AFV60	Lecco Line, Western Branch	Norian Carbonate Platform (Dolomia Principale)	Moregallo Unit (U3)	45.8837	9.3275	c.1	Dolomit e	Vein cut with a high cutoff angle by dextral slickenfiber	Unimodal, planar-e	13.5 ± 0.7
AFV144	Lecco Line (Monte Barro)	Lower Jurassic, syn-rift (Moltrasio Lms.)	Canzo Unit, Flessura Pedemontana (Ub)	45.8287	9.3718	d.1	Calcite	Dextral slickenfibers	Blocky	60.2 ± 10.1
AFV8	Lecco Line (Rocca Innominato)	Lower Cretaceous (Maiolica)	Innominato Unit, Flessura Pedemontana (U4)	45.8157	9.4268	e.1	Calcite	Vein related to a strike-slip fault system. Crack-and-seal event.	Blocky	8.7 ± 6.7
						e.2	Calcite	Parallel vein, reopening a older stylolite.	Blocky	69 ± 34
Thrust-related dated carbonates										
AFV192	Grigna-S Thrust	Lower Triassic Units (Prezzo Lms.)	Grigna S Unit (U1.5)	45.9166	9.3985	1.1	Calcite	Bed-parallel vein	Blocky	105.2 ± 9.2
						1.2	Calcite	Bed-parallel vein	Blocky	92 ± 13
AFV90	Due Mani Thrust	Norian Carbonate Platform (Dolomia Principale)	Due Mani Unit (U2)	45.8806	9.4379	2.1	Dolomit e	Bed-perpendicular vein	Unimodal, planar-s	84.8 ± 8.6
AFV119	Due Mani Thrust	Norian Carbonate Platform (Dolomia Principale)	Due Mani Unit (U2)	45.8808	9.4380	3.1	Dolomite	Dolomite-Cemented Breccia	Unimodal, planar-s	213 ± 11
AFV143_3	Monte Barro, Lower Thrust	Lower Jurassic, syn-rift (Moltrasio Lms.)	Canzo Unit, Flessura Frontale (Ub)	45.8287	9.3718	4.1	Calcite	High angle vein cut by slickenfiber (4.2)	Blocky	33.5 ± 7.2
						4.2	Calcite	Reverse Slickenfibers	Fibrous	31.4 ± 6.4
						4.3	Calcite	High angle vein cutting the slickenfiber (4.2)	Blocky	11.2 ± 3.3
						4.4	Calcite	Reverse Slickenfibers, younger sheet	Blocky	9.1 ± 4.2
AFV73	Neguccio Thrust, splay of Lecco Thrust	Rhaetian (Zu Lms.)	Innominato Unit, Flessura Frontale (U4)	45.8479	9.4199	5.1	Calcite	Along foliation vein (older)	Fibrous to blocky	114 ± 20
						5.2	Calcite	Along foliation vein (younger) cutting 5.1	Blocky	95.6 ± 4.3
AL-9	Albenza Anticline	Rhaetian (Zu Lms.)	Albenza Unit, Flessura Pedemontana (UII.I)	45.7651	9.5581	6.1	Calcite	Slickenfiber cutting folded strata	Blocky	37.1 ± 4.4

Note. They've been distinguished between mineralizations collected along thrusts and TZs. Tectonic units are from Figure 2b. Coordinates are given in WGS 84. Habitus classifications are from Bons et al. (2012) for calcite and from Sibley and Gregg (1987) for dolomites.

overlapped sheets of calcite (d.1), which are bounded by pressure-solution seams. Blocky calcite with homogeneous red luminescence characterizes these fibers. They yielded an age of 60.2 ± 10.1 Ma, related to fault slip.

Sample AFV8 (Figure S10 in Supporting Information S1), collected at Rocca dell'Innominato in Lower Cretaceous limestones, belongs to the FP structure (Figure 12). Veins are oriented parallel to the main strike-slip faults of the Lecco Line fault zone and are surrounded by tension gashes, suggesting that they developed under a shear-dominated deformation regime. In thin section, they preserve evidence of crack-and-seal events, as shown by the precipitation of younger calcite increments (e.1) within a large vein. Older calcites (e.2) filling re-opened stylolites are crosscut by these veins. Both generations of veins are composed of blocky calcite and are dull red under CL. Phase e.1 yielded an age of 8.7 ± 6.7 Ma, constraining the timing of calcite precipitation during crack-and-seal processes. Phase e.2 yielded an older age (69 ± 34 Ma). The large analytical uncertainty limits its tectonic significance and provides only clues of earlier deformation.

4.2.3. Thrusts—Internal Belt

AFV192 (Figure S11 in Supporting Information S1) has been sampled in the hanging wall of the Grigna-S Thrust (Thrust sheet 1, Figures 2a and 12). It consists of N-dipping, bed-parallel veins within upper Anisian-Ladinian limestones. In thin section, a major bed-parallel vein has been observed (1.1), intersecting a thinner one at ∼20–30° (1.2). Blocky calcites characterize both veins. Under CL, the thicker vein is moderately bright, while the thinner one is non-luminescent. Vein 1.1 yielded an age of 105.2 ± 9.2 Ma, and vein 1.2 an age of 92 ± 13 Ma, constraining the timing of calcite precipitation in low-angle contractional fractures in the hanging wall of Grigna-S Thrust.

Sample AFV90 (Figure S12 in Supporting Information S1) has been collected five m above the main surface of the DMT, within thrust sheet 2 (Figures 2a and 12). It consists of NNE-SSW, bed-perpendicular veins within Norian Dolostones with similar orientation to the oblique faults recorded in the fault zone. They are almost perpendicular to the thrust plane (Figure S6c in Supporting Information S1). They are interpreted as the product of opening and subsequent sealing of fractures under conditions of high fluid pressure in the hanging wall of the thrust. These veins are characterized by several crack-and-seal events, which indicate multiple reopening and precipitation of later carbonate phases. Veins are composed of unimodal, planar-s dolomite and are dull under CL. One of the crack-and-seal events (2.1) yielded an age of 84.8 ± 8.6 Ma.

Sample AFV119 (Figure S13 in Supporting Information S1) comes from the hanging wall Norian dolostones of the DMT, within thrust sheet 2 (Figures 2a and 12). It is a fault rock collected from an oblique, NW-verging fault (Figure 10c) located 10 m above the main thrust surface and decorated by cataclasite. In thin section, ultracataclasite characterizes the fault core, separated from fractured and brecciated dolostones by sharp surfaces. Dolomite-cement (3.1) fills voids created by fracturing and brecciation of the host rock, and is characterized by a unimodal, s-planar habitus, and displays CL zonation. 3.1 yielded an age of 213 ± 11 Ma, constraining the timing of cement precipitation following fracturing and brecciation interpreted as fault-related, rather than discrete slip. The very high MSWD (=25) is due to significant variations in initial lead. Considering recorded variations in initial lead content (0.4–0.6), it would result in age differences below 1%. However, the high MSWD still indicates significant scatter and associated uncertainty in the age.

4.2.4. Thrusts—Flessura Pedemontana

Sample AFV143_3 (Figure S14 in Supporting Information S1) has been collected 15 m beneath the main fault plane of the Monte Barro Lower Thrust, within Lower Jurassic syn-rift units (Figures 9f and 12). The sample consists of slickenfibers developed on a reverse fault plane. Some high-angle veins (4.1) are crosscut by the slickenfiber (4.2) at an angle of ∼70°, whereas other veins (4.3) cut it perpendicularly. The slickenfiber is characterized by several overlapping sheets; on the right margin of the thin section, a younger generation of stepped calcite overprints the slickenfiber (4.4). A tooth-shaped, calcite vein occurs at the right edge of the thin section. The high-angle veins (4.1 and 4.3) are composed of blocky calcite and are dull under CL. The slickenfiber is composed of fibrous calcite and is dull under CL. The stepped calcite exhibits blocky texture and CL zonation. Vein 4.1 yielded an age of 33.5 ± 7.2 Ma and 4.3 yielded an age of 11.2 ± 3.3 Ma, not unequivocally associated with faulting. The slickenfiber (4.2) yielded an age of 31.4 ± 6.4 Ma and records fault-related slip. The younger stepped calcite (4.4), developed along the fault plane, yielded an age of 9.1 ± 4.2 Ma and reflects a late stage of syn-kinematic calcite growth.

10.1029/2025TC009200

Sample AFV73 (Figure S15 in Supporting Information S1) has been collected along the Neguccio Thrust, a footwall-splay of the LT, part of the FP structure (Figure 12). Calcite precipitated along shortening-related S-C foliation in Rhaetian marly horizons, just below the thrust surface. In thin sections, we recognize several generations of veins along foliation planes, showing crosscutting relationships which define their relative ages. Two of them yielded interpretable ages. The oldest veins (5.1) are characterized by blocky to fibrous calcite and are dull under CL. Younger veins crosscut the older ones along contractional foliation, displaying a higher angle (5.2); they exhibit blocky texture and are dull under CL. Sample 5.1 yielded an age of 114 ± 20 Ma and vein 5.2 an age of 95.6 ± 4.3 Ma, constraining the timing of calcite precipitation along contractional foliation.

Sample AL9 (Figure S16 in Supporting Information S1) consists of calcite slickenfibers sampled along a mesoscopic dip-slip thrust plane (Dip direction/dip: 235°/47°; 028°) crosscutting steep, almost vertical, bedding striking NW–SE in the Rhaetian marly limestones of the forelimb of the eastern FP (Figure 12). Calcite displays a blocky to elongated-blocky habitus, with sub-micrometric crystals, and is dull red under CL. Several overlapping sheets are marked by solution cleavage planes. Calcite slickenfibers (6.1) crosscut high-angle veins filled with elongated-blocky calcite, displaying a dull-red luminescence. Calcite slickenfiber (6.1) yielded an age of 37.1 ± 4.4 Ma and records slip along a low-angle thrust fault plane crosscutting previously steepened bedding. The high-angle veins did not yield interpretable ages.

5. Discussion

The following discussion focuses on the pre-orogenic origin, compressional reactivation, and tectonic role of the TZs during shortening in the CSA and the timing of fault-related deformation. In particular, we discuss how the reactivation of inherited faults as TZs may be related to the accommodation of differential shortening rates along strike within the fold-and-thrust belt (Boyer & Elliott, 1982) and how this process may be controlled by stress rotations and/or permutations (Peacock et al., 2017; Tavani et al., 2015).

The age of thrust faulting will also be discussed, refining previous tectonic interpretations of the CSA.

5.1. Pre-Orogenic Origin of Transverse Zones

Geochronological and mesoscale analyses are consistent with a pre-orogenic origin for TZs and indicate that some thrusts originated as rift-related extensional faults that were later positively inverted. In this section, we discuss each pre-orogenic tectonic phase identified in the study area, and evaluate which faults were inherited from these phases and later evolved into TZs (Figure 14a).

5.1.1. Permian

The earliest evidence of pre-orogenic faulting affecting the CSA is Permian in age and is documented in the northern Orobic chain (Locchi et al., 2022; Pohl et al., 2018; Zanchi et al., 2019). E–W striking faults developed under a transtensional to purely extensional stress regime associated with post-Variscan tectonics (Locchi et al., 2022; Pohl et al., 2018). No direct evidence of Permian tectonics is preserved in the study area, where Mesozoic rocks are predominantly exposed. However, the E–W strike of Permian faults contrasts with the N–S orientations of the Southalpine TZs. In principle, E–W striking faults could have been reactivated as thrust faults during N–S Alpine shortening in the inner portions of the belt (e.g., Valtorta and the Valsassina Line; Locchi et al., 2022; Schönborn, 1992), but were unfavorably oriented for reactivation as strike-slip or transpressional faults, such as the TZs (Thomas, 1990).

5.1.2. Ladinian

Although no regional evidence for a Ladinian tectonic phase is reported in the literature for the CSA, a coeval phase has been widely documented in the ESA (Dolomites; Doglioni & Carminati, 2008). Similar to the CSA, in this period the Dolomites were characterized by progradation of carbonate platforms onto adjacent pelagic basins. However, Middle Triassic faults, widespread in the Dolomites area, remain elusive within the Lombardy Basin (Berra et al., 2011). In this area, Middle Triassic tectonics has been suggested to explain variable subsidence and lateral facies changes between Late Anisian and Ladinian times (Brack & Rieber, 1993; Gianotti, 1984). In the study area only local N–S Ladinian syn-sedimentary faults were recognized (in the Lierna area; Figures 6a–6c, 13, and 14), insufficient to support widespread coeval tectonics. Possibly, these minor structural discontinuities, combined with the rheological contrast between shallow-water and pelagic carbonates, may have served as zones of mechanical weakness along which deformation was localized during subsequent pre- and syn-orogenic tectonic phases (Figure 14a). This is suggested by the parallelism between TZs/thrust faults and Middle Triassic facies changes (Figure 5a).

5.1.3. Late Norian

The occurrence of N–S and E–W late Norian normal faults, generating intraplatform rift-related basins, has already been suggested on stratigraphic grounds (Berra & Jadoul, 1996; Jadoul et al., 1992). These structures represent the oldest faults reactivated as TZs during the orogeny. The late Norian N–S striking faults correspond to first-order (e.g., Faggio Line) and second-order TZs (e.g., Val Fontana Fault, Riva Foppa-Fo TZ, Monte Linzone Fault, RT; further details and previous interpretations are provided in Text S3 and S4 in Supporting Information S1; Figures 5b and 14b). N–S striking faults are the major Late Norian tectonic structures and accommodated a general eastward deepening of the paleobathymetry and increase in tectonic subsidence. Notably, the Faggio Line marks the most abrupt change in thickness of the upper Norian basinal rocks, separating the Valle Imagna Basin from the Resegone Platform (Figure 5b). Late Norian E–W-striking faults (e.g., Due Mani Fault, Balisio Fault, Imagna Fault; Figure 5b) are generally located between major N–S-striking faults and likely acted as relay-ramps or releasing faults (Destro, 1995). A pre-orogenic origin of the DMT is also supported by the following features shown in Section 4.1.1: (a) younger-on-older relationships; (b) occurrence of Late Norian basinal deposits in the hanging wall; (c) beheading of a rift-related normal fault system and its passive transport during later shortening; (d) the presence of meso-scale E–W striking rotated normal faults, partly reactivated (Figure 10; S6 in Supporting Information S1). In this framework, our U–Pb data provide additional temporal constraints. In particular, an age of 213 ± 11 Ma (sample AFV119, 3.1; Figures 12 and 13), obtained from dolomite-cemented breccia within the DMT fault zone, records brecciation and cement precipitation within the fault damage zone. Although affected by significant scatter, this age provides supportive evidence for Late Norian tectonic activity and is compatible with a pre-orogenic origin of this structure.

5.1.4. Early-Middle Jurassic

It is widely accepted that an Early-Middle Jurassic rifting phase strongly influenced the tectono-stratigraphic architecture of the study area (Berra & Carminati, 2010; Rocca et al., 2024; Santantonio & Carminati, 2011), promoting the development of major N–S striking normal faults and partly reactivating pre-existing Late Norian structures (Figures 5c and 14b). Toarcian?–Aalenian? ages (173.7 ± 2.4 Ma, sample AFV4, a.1; Figures 12 and 13) of subvertical veins record fracture opening and sealing within the fault zone of the Faggio Line (Figure 8f). This age agrees with Early Jurassic activity of the line, previously proposed on stratigraphic grounds (Jadoul & Doniselli, 1986). Similar U–Pb ages from syn-tectonic carbonates of the Amora Fault System (Figure 1b), located ca. 20 km further east, were recently reported by Rocca et al. (2024, 2026). In the southern part of the fault, no evidence of Early Jurassic tectonic activity is found. For instance, no abrupt thickness changes are observed across the fault between the Lecco Basin and the Albenza Plateau (Figure 5c).

The Lecco Line bounds the Canzo High, that is, the eastern termination of the Monte Generoso half-graben. In the Early Jurassic, this fault system consisted of an east-dipping master fault to the west and a west-dipping antithetic fault to the east, bounding the intervening Moregallo Corridor (Figure 5c). The syn-rift succession exposed in the hanging wall of the Lecco Line (Lecco Basin) reaches its maximum thickness to the east of the fault (Figures 5c and 6e) and progressively thins toward the Albenza Plateau. This geometry suggests the existence of an Early Jurassic N–S oriented half-graben in the hanging wall of the Lecco Line (Bertotti et al., 1993).

Although subordinate to the major N–S-striking structures, some present-day E–W-striking faults played a significant role in shaping the Early Jurassic paleogeography of the study area, as evidenced by the thickness changes of syn-rift sediments across these structures. The most prominent E–W-striking Early Jurassic structures are the Canzo Fault, the Imagna Fault, and the fault separating the Albenza High from the Gerola Basin (Figure 5c).

In summary, structural and stratigraphic observations, supported by geochronological constraints derived from exposed TZs and thrust-fault zones, suggest a significant pre-orogenic component for the origin of these

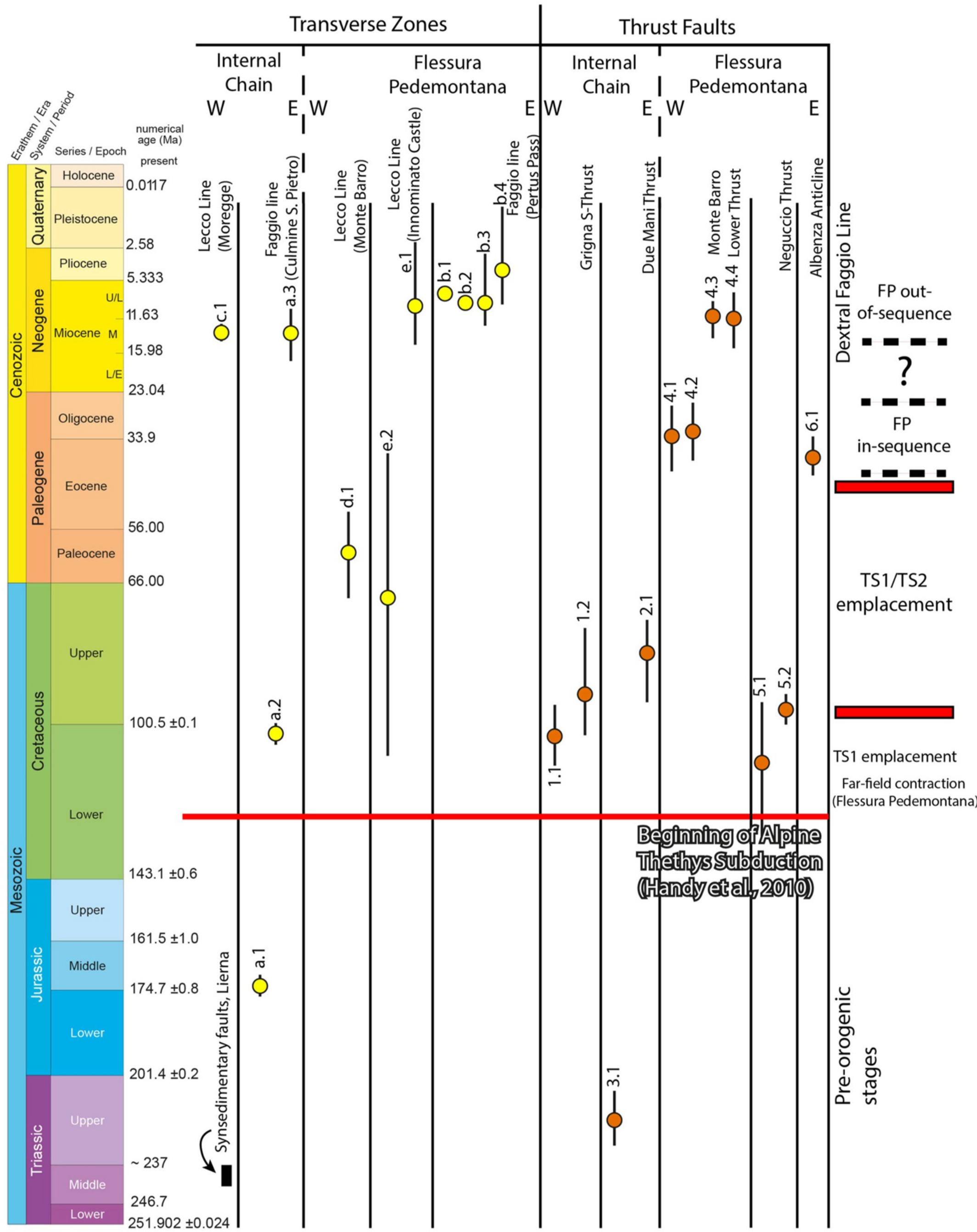

Figure 13. Chronological scheme showing U–Pb absolute ages obtained from the northernmost, internal part of the chain and from the Flessura Pedemontana, toward the frontal zone of the belt. Yellow dots represent mineralizations sampled along Transverse zones, while orange dots those sampled along thrust faults. Data are arranged from west to east within each sector. The onset of Alpine Tethys subduction is from Handy et al. (2010). TS1/TS2: Thrust sheet 1/2. FP: Flessura Pedemontana. Chronostratigraphic chart is from ICS, version 2024/2012.

structures (Figure 14b). Alpine tectonics subsequently overprinted and dismembered the pre-orogenic tectono-stratigraphic architecture, complicating any regional reconstruction of the Mesozoic faults (Figures 14a and 14b). In the study area, E–W extension accommodated by major N–S striking faults led to the formation of N–S elongated basins. However, E–W striking faults, although subordinate, played a significant role in shaping the syn-rift structural architecture of the CSA.

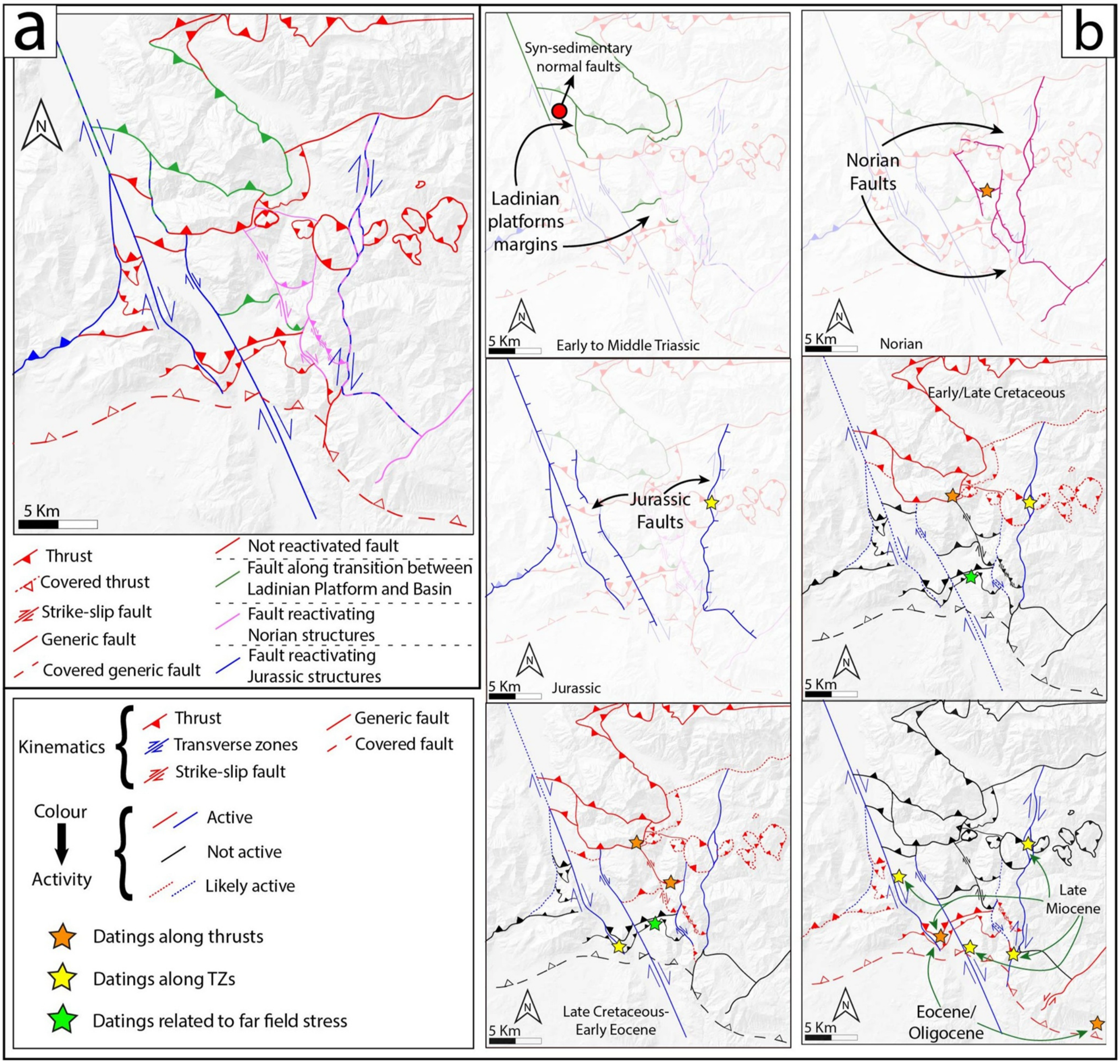

Figure 14. Schemes summarizing the tectonic evolution of the study area. (a) Present-day major faults of the study area. Different colors indicate the age of the reactivated pre-orogenic structures. (b) Tectonic evolution of the study area, starting from pre-orogenic throughout the syn-orogenic stages. The panels show the faults activated during the different stages and the radiometric ages that constrain such activations. Legend of the colors of the faults reported in Early to Middle Triassic, Norian, and Jurassic panels are shown in panel (a).

5.2. Syn-Orogenic Reactivation of TZs

In this section, we discuss the timing of reactivation (based on U–Pb ages of syn-tectonic carbonates), the geometries and relative kinematics observed in TZs and the positive inversion of inherited E–W striking normal faults.

5.2.1. Faggio Line

Along the northern Faggio Line, dextral transpressional shear planes cutting Lower Jurassic subvertical veins are filled by two generations of blocky to fibrous calcite, yielding ages of 103.2 ± 2.2 Ma (a.2) and 13.1 ± 4.5 Ma (a.3) (Sample AFV4; Figures 11–13). These mineralizations record crack-and-seal processes associated with shear deformation (Roberts & Holdsworth, 2022). Dating of calcite slickenfibers from the southern portion of the Faggio Line (Pertus Pass) indicates Tortonian dextral strike-slip fault motion in this sector (b.1: 7.1 ± 0.2, b.2: 7.9 ± 0.2, b.3: 7.9 ± 4.7; sample AFV105; Figures 12 and 13). These Cretaceous and Miocene U–Pb ages of syn-tectonic mineralizations suggest recurrent deformation and mineral precipitation associated with reactivation of the Mesozoic Faggio Line (Figures 13 and 14a).

Kinematic indicators (i.e., the coexistence of dextral and sinistral meso-scale fault slip indicators within the fault zone, Figure 8b, Figure S4j in Supporting Information S1), contrasting paleostress reconstructions (Figure 8b, Figures S4e–S4h in Supporting Information S1) and regional-scale observations (e.g., the indentation-like geometry of the Resegone–Camozzera units, Figure 2b), suggest a complex strike-slip to transpressional kinematics, characterized by changes in slip sense through time for the Faggio Line. Unfortunately, owing to scattered and discontinuous outcrops, to the lack of unequivocal cross-cutting relationships, and to the absence of sufficient U–Pb ages, the timing of such changes cannot be tightly reconstructed. Time constraints are available only for dextral (Miocene, b.1: 7.1 ± 0.2, b.2: 7.9 ± 0.2, b.3: 7.9 ± 4.7 Ma for sample AFV105) and not for sinistral shear.

In addition to our geochronological constraints, late Cenozoic dextral slip along the Faggio Line is supported by structural evidence. Mesoscale kinematic indicators consistently suggest dextral slip in the southernmost sector, and paleostress reconstructions from this area suggest a NE–SW oriented maximum principal stress axis (Figure S4h in Supporting Information S1). Dextral kinematics was also observed along the main fault planes in the internal portions of the line (Figures 8c and 8d; Figure S4i in Supporting Information S1). The Miocene dextral slip along the Faggio Line is consistent with the development of the frontal thrust system (FP), independently constrained by U–Pb ages (4.3: 11.2 ± 3.3; 4.4: 9.1 ± 4.2 Ma; sample AFV143_3; Figures 12–14). The dextral bending of the Albenza Anticline (Figures 2, 3a, 13, and 14b) is consistent with this kinematic framework. NW–SE trending en échelon folds occurring east of the Resegone unit along the Faggio Line in the Upper Triassic to Jurassic units as well as the synform structure bending the Maesimo klippe also suggest dextral shearing along the fault zone (Gaetani et al., 2012; Figure S4k in Supporting Information S1).

5.2.2. Lecco Line

Along the Lecco Line, dextral strike-slip deformation was directly constrained to the Late Cretaceous?/Paleocene? by an age obtained from a slickenfiber (60.2 ± 10.1 Ma; sample AFV144, d.1; Figures 12 and 13). Miocene/Pliocene? fracture sealing and damage-zone mineralization are recorded by veins (13.5 ± 0.7 Ma, sample AFV60, c.1; 8.7 ± 6.7 Ma, sample AFV8, e.1; Figures 12 and 13); their relationship to slip is indirect. Sample AFV8 also preserves an older vein yielding an age of 69 ± 34 Ma (e.2, Figures 12 and 13), which is crosscut by the younger one (Figure S10 in Supporting Information S1). This is indicative of an earlier phase of deformation, poorly constrained due to the large analytical uncertainty. During the Alpine orogeny, the reactivation of the Lecco Line involved both branches of the Lower Jurassic normal fault system (Figures 5c and 14). Contractional structures developed between these two branches, including folds (at Mt. Moregallo; Agliardi & Crosta, 2014), thrusts (at Mt. Barro and Abbadia Lariana; Schönborn, 1992) and positive flower structures (this study, Figure 9d). This structural assemblage is consistent with the development of a restraining stepover, which does not correspond to a present-day topographic high because the fault-damaged and therefore more erodible area was preferentially eroded by glaciers that formed the Como Lake depression, possibly flowing along pre-existing Messinian valleys (Bini et al., 1978). Overall, the Lecco Line shows consistent dextral kinematic indicators along its entire length (Figure 9), compatible with reactivation of the pre-orogenic NW–SE oriented fault zone under a NNE–SSW maximum principal paleostress axis (Figures 9b and 14, Figure S5d in Supporting Information S1). No evidence of a kinematic switch has been documented along the line.

5.2.3. Positive Inversion of Inherited E–W Striking Normal Faults

Along with N–S faults, we suggest that also inherited Mesozoic E–W striking normal faults were reactivated during shortening (Figure 14a). NNE-SSW, bed-perpendicular veins in the hanging wall of the N-dipping DMT yielded ages of 84.8 ± 8.6 Ma (sample AFV90, 2.1; Figure 12), consistent with fracturing and sealing within the fault damage zone during Late Cretaceous compressional stages (Figure 14b). This indirectly supports the positive inversion of the Upper Norian Due Mani Fault under NW–SE oriented shortening (Figures 12–14). The occurrence of thrusting-related S-C foliation within the fault zone, indicating a SE-directed transport, corroborates the syn-orogenic reactivation of this fault, along with the occurrence of tilted normal faults showing reverse slickenfibers and associated folds (Figures 10b, 10d, and 10e). Other E–W pre-orogenic (Late Norian and Early Jurassic) faults were likely reactivated during the orogenic stages (e.g., Monte Bollettone Thrust, Figures 5c and 14a). Such positive inversion of well-oriented pre-orogenic normal faults has been generally overlooked in the CSA, where previous paleogeographic reconstructions have primarily focused on major N–S-striking pre-orogenic structures.

In summary, structural analyses and U–Pb ages of syn-tectonic mineralizations (slip- or sealing-related) are consistent with the repeated reactivation of the N–S Mesozoic pre-orogenic extensional faults during Alpine shortening with a major strike-slip component. Reactivation is interpreted to have occurred under an overall ~N–S maximum principal paleostress axis, which possibly shifted over time (and possibly in space) between NW–SE and NE–SW orientations. Consequently, NW–SE–striking inherited faults (e.g., Lecco Line) were reactivated as dextral strike-slip faults, whereas the N–S faults (e.g., Faggio Line) were possibly reactivated with variable senses of slip through time. Structural inheritance, including fault undulations and en-échelon geometries, guided the development of restraining bands within the main TZs (Lecco and Faggio Lines). We suggest that some N-dipping rift-related normal faults were positively inverted in agreement with a paleostress field with a roughly N–S maximum principal axis.

5.3. Role of Transverse Zones During Shortening

Building on previous discussions, we propose that TZs are not merely inherited boundaries but can represent ancestral anisotropies that: (a) partition strain along strike between adjacent domains; (b) segment and link thrust systems; (c) localize shortening and vertical-axis rotations, thereby influencing the 3D architecture of the belt; (d) accommodate deformation at different stages of wedge development.

1. Along-strike strain partitioning in the CSA reflects the interactions between Alpine shortening and the inherited, rift-related tectono-stratigraphic architecture (e.g., Zanchi et al., 2012). During the orogeny, deformation was accommodated predominantly by thrusting and folding within individual structural blocks, whereas oblique-slip and transpressional strain was preferentially localized along the TZs. Furthermore, lateral variations in stratigraphy and pre-orogenic faults controlled lithological competence and depth of décollements, which, in turn, influenced the development of thrust-ramp geometries versus décollement folding, thereby enhancing along-strike contrasts in structural style (e.g., Mazzoli et al., 2022; Figures 2–4; Text S1 in Supporting Information S1). In fact, fold-dominated shortening characterizes the Monte Generoso sector, where Lower Jurassic syn-rift strata attain their maximum thickness and overlie an Upper Norian basinal unit that likely acted as an effective décollement. In contrast, thrust-dominated shortening characterizes the Grigne–Valsassina sector, where mainly competent and thick Ladinian and Upper Norian carbonates were incorporated into the thrust system. By contrast, the Aralalta–Albenza sector is a structural plateau overlain by small klippen, consistently with the involvement of thick Upper Norian shales, which acted as an effective décollement. The positive inversion of pre-orogenic N-dipping normal faults, laterally confined between TZs (e.g., DMT), further supports the idea that inherited, TZ-bounded architecture compartmentalized deformation and shaped the syn-orogenic structural assemblage (Figures 4a, 7c, 14a; Schönborn, 1992).
2. Furthermore, the kinematics and geometry of primary and secondary TZs promote hard linkage and segmentation of thrust traces (Rocca et al., 2026; Zanchi et al., 2012). This is illustrated by the southward segmentation and progressive exposure of the thrusts bounding thrust sheets 2 and 3, which are dissected by a system of dextral TZs (Figures 2a and 7b). Major thrust surfaces may also link and merge across TZs (e.g., Qayyum et al., 2015). For example, the Lecco (purple in Figure 2a) and Coltignone (black in Figure 2a) thrusts are clearly distinguishable west of the Riva–Foppa TZ, whereas east of this TZ they merge into a single major thrust surface (colored black and purple in Figure 2a) that separates thrust sheet 2 from the FP.
3. TZs also accommodated vertical-axis rotations and lateral ramping. For example, the along-strike continuous FP structure displays apparent rotation of up to ~60°, and an increase in strain and kinematic complexity approaching the TZs (Section 4.1.2; Schönborn, 1992). In detail, the regional-scale bending of the FP east of the Faggio Line (Figures 2 and 3a), suggests lateral ramping and near-vertical axis folding along this TZ, consistent with non-negligible shortening accommodation. As highlighted by analogue models (e.g., Calassou et al., 1993), shortening within thicker sedimentary sequences is accommodated by fewer thrusts and results in a faster advance of the orogenic front. This observation is compatible with the (Late?) Cenozoic dextral kinematics of the Faggio Line, considering the larger frontal advancement of the eastern sector, where thicker

syn-rift deposits occur and fewer thrust faults are exposed. Between the Faggio and Lecco Lines TZs, the overturning of the forelimb of the FP increases (Figures 6e and 9a), and the forelimb is dissected by the LT system (Figures 2b, 3a, 4a, 6e). West of the Lecco Line (Figure 9a), the FP is again characterized by an anticline with a vertical to overturned forelimb.

4. The timing of activity of thrusts and TZs also provides further significant information. The Faggio Line records broad temporal overlap with along-strike thrust faults (e.g., a.2 with 1.1 and 1.2; a.3 and b.1–b.4 with 4.3 and 4.4; Figure 13). This is also consistent with mutual cross-cutting relationships between strike-slip and reverse faults observed along the Lecco Line at Monte Barro (Section 4.1.2). However, significant exceptions occur: Miocene fault-related deformation along the Lecco and Faggio Lines TZs is recorded in internal sectors where shortening is mainly Cretaceous (Zanchetta et al., 2015), whereas Late Cretaceous–Paleogene slip along the Lecco Line occurs in the external sector, where deformation is largely post-Eocene (Schönborn, 1992; Fantoni et al., 2004; Figure 13). This spatial–temporal decoupling suggests that TZ activity does not necessarily track a simple piggyback sequence of thrust propagation. Analogue models suggest that inherited discontinuities orthogonal or oblique to thrust fronts may localize deformation early in the foreland, consistent with the early activity of the Lecco Line. Moreover, within a thickened wedge, strain may be initially distributed and only later localized into discrete TZs depending on wedge strength and boundary conditions (Toscani et al., 2009), explaining the late activation of TZs in the internal zones.

From a qualitative perspective, the CSA exhibit a structural architecture influenced by the TZs, which play a role in controlling structural style, strain partitioning and localization. However, a unique role for these faults is unlikely: processes such as displacement transfer (Dahlstrom, 1970) or strike-slip faulting related to stress permutations during thrust stacking (Peacock et al., 2017) may localize along these structures, without necessarily exerting a dominant control on the overall architecture of the CSA. Quantifying the relative contribution of these processes requires further investigation, including structural restorations, sector-by-sector shortening comparisons, and independent tests for vertical-axis rotation.

5.4. Tectonic Evolution of the Southern Alps

We now discuss, in the framework of the evolution of the Southern Alps retrobelt and the Alpine-Mediterranean area, the significance of tectonic phases constrained by our U–Pb ages (Figure 14b).

Concerning rift-related tectonics, evidence for Late Triassic and Early Jurassic ca. N–S extensional faults is widespread in the Adria plate (e.g., Southern Alps, Bertotti et al., 1993; Adriatic sea and Apennines, Santantonio & Carminati, 2011) and is related to divergence between the Adria and European plates. These faults led to the development of coeval asymmetric fault-bounded rift basins and laterally heterogeneous passive-margin sequences (Dal Piaz et al., 2003), followed by the opening of the Alpine Tethys ocean (Handy et al., 2010).

The rift-related N–S faults were then reactivated as TZs during the following contractional deformation, related to the convergence between the Adria and Europe that initiated in Early Cretaceous time (Handy et al., 2010). The Early Cretaceous ages (Figures 12 and 13) obtained from syn-tectonic carbonates of the Faggio Line (a.2: 103.2 ± 2.2 Ma) and the GTS (1.1: 105.2 ± 9.2 Ma; thrust sheet 1) are consistent with regional evidence for Aptian-Albian shortening provided by the onset of foredeep sedimentation in both the CSA and the ESA (Bernoulli & Winkler, 1990; Bersezio et al., 1993; Castellarin et al., 2006; Doglioni & Bosellini, 1987; Rožič, 2005; Figure 14b), likely following the onset of Alpine Tethys subduction (Handy et al., 2010). Early Cretaceous shortening also occurred in the eastern Austroalpine domain of the Alps, north of the Periadriatic Lineament (Ratschbacher, 1986).

Late Cretaceous-Paleogene ages (Figures 12 and 13) from syn-tectonic carbonates of the GTS (1.2: 92 ± 13 Ma; thrust sheet 1), the Due Mani-Coltignone Thrust (2.1: 84.8 ± 8.6 Ma; thrust sheet 2) and the Lecco Line (d.1: 60.2 ± 10.1 Ma) are consistent with structural (D'Adda et al., 2011), geochronological (Zanchetta et al., 2011) and sedimentological (Bersezio et al., 1993) constraints previously reported for the CSA (Zanchetta et al., 2015) and with geochronological ages from the ESA (Curzi et al., 2024). Cretaceous deformation in the CSA has been interpreted (e.g., Zanchetta et al., 2012, 2015) as the expression of a shortening and stacking phase (Eo-Alpine, Cretaceous-Early Eocene; Figure 14b) of the Alpine belt during pre-collisional stages (Handy et al., 2010), whereas that in the ESA reflect foreland propagating deformation associated with far-field shortening (Curzi et al., 2024). The Cretaceous U–Pb ages 114 ± 20 and 95.6 ± 4.3 Ma (sample AFV73, 5.1, 5.2; Figures 12 and

13), obtained from veins bounding contractional foliation in the FP (whose main structuration is Cenozoic, as detailed below), may suggest that far-field shortening also occurred in the CSA (Figure 14b).

Two Cenozoic U–Pb ages (sample 6.1: 37.1 ± 4.4 Ma; sample 4.2: 31.4 ± 6.4 Ma; Figure 13) from reverse slickenfibers cutting upright beds of the FP are consistent with an Eocene?-Oligocene? build-up stage in this part of the CSA (Figure 14b), related to the broadly coeval collision between Adria and Europe (Handy et al., 2010). This is consistent with the evidence for uplift and erosion of the Mesozoic succession of the CSA as recorded by Upper Eocene-Oligocene syntectonic sediments of the Gallare-Aveto Group (Bernoulli et al., 1987; Di Capua et al., 2016; Di Giulio et al., 2001; Zanchetta et al., 2015). In the ESA, Oligocene-Early Miocene shortening has been previously recorded from U–Pb ages of slickenfibers along the Belluno and Valsugana Thrusts (Curzi et al., 2024), and from related syn-contractional deposits (Castellarin et al., 1992). This thrusting stage encompasses the onset of the Adria–Europe collision following the closure of the Alpine Tethys (Handy et al., 2010).

A Late Miocene contractional stage is recorded by U–Pb ages from syn-tectonic carbonates in the FP (4.3: 11.2 ± 3.3 Ma; 4.4: 9.1 ± 4.2 Ma; Figure 13), and along the Lecco (e.1: 8.7 ± 6.7; c.1: 13.5 ± 0.7; Figure 13) and Faggio Lines (a.3: 13.1 ± 4.5 Ma; b.1: 7.1 ± 0.2 Ma; b.2: 7.9 ± 0.2 Ma; b.3: 7.9 ± 4.7 Ma; Figure 13). These ages overlap, within uncertainty, with the timing of deformation farther south in the Milano Belt. There, thrusts faults deform Lower and Middle Miocene sediments (Cassano et al., 1986; Pieri & Groppi, 1981) buried under the Po Plain; this temporal overlap may reflect either out-of-sequence reactivation or more distributed/synchronous shortening (Curzi et al., 2025; Figure 14b), but the present data do not allow distinguishing between these alternatives. However, Miocene out-of-sequence thrusting in the FP was previously proposed based on surface and subsurface geological data (Fantoni et al., 2004; Schönborn, 1992). Late Miocene thrusting is also well known in the western CSA, as testified by the backthrusting of the Gonfolite wedge (Bernoulli et al., 1989).

Collectively, our data suggest a two-phase tectonic evolution of the FP: an in-sequence phase in the Eocene?-Oligocene? and a final out-of-sequence/synchronous phase in the Late Miocene, whereas previous works interpreted it as a single-stage out-of-sequence structure (Schönborn, 1992). The implications of this revised timing for the geometry of thrusts and folds in the area are discussed in Figure 4a and in Text S6 in Supporting Information S1. In the ESA, Late Miocene tectonics is recorded by syn-thrusting deposits up to 1,500 m thick (Castellarin et al., 1992 and references therein), ∼10 Ma exhumation ages for the basement units in the hanging wall of the Valsugana Thrust (Zattin et al., 2006) and U–Pb ages of calcite slickenfibers from the same structure (Curzi et al., 2024). Late Miocene thrusting in the CSA was synchronous with deformation in the Western Subalpine (∼15–8 Ma, Bilau et al., 2023) and Jura Mountains (∼14–4 Ma, Looser et al., 2021; Smeraglia et al., 2021), as well as with strike-slip and extensional activity along the Penninic front (Bilau et al., 2025) and within basement units of the Western and Central Alps (Ceccato et al., 2024; Rolland et al., 2009). These deformations indicate a belt-scale Miocene event from ∼15–14 to ∼5 Ma (Rolland et al., 2022), linked to NW-directed push of Africa (Le Breton et al., 2017), and Adria indentation in the Eastern and Western Alps (Schwartz et al., 2024; Verwater et al., 2021).

Finally, we speculate that the Late Miocene reactivation of the FP structure and the Gonfolite backthrust could indicate a wedge-scale internal readjustment of the CSA, promoted by enhanced unroofing of the internal part of the belt and by coeval foreland loading and sedimentation in the Po Plain. The Apennines subduction and the interplay between the Alps and Apennines belts could have played a role as well. According to several reconstructions (e.g., Carminati et al., 2010; Faccenna et al., 1997), the Apennines subduction system started to retreat radially from late Eocene-early Oligocene time and the northern part of the Apennines belt front migrated progressively to the NE, toward the Southern Alps. In the central part of the Po plain area, the two belts interacted (Figure 1a) and the Apenninic peripheral arches reached and deformed the southern part of the CSA, possibly inducing out-of-sequence thrusting at the mountain front.

5.5. Transverse Zones Persistence: Comparison With Other Fold-and-Thrust Belts Worldwide

Thomas (1990) was among the first to review and classify TZs within fold-and-thrust belts, identifying several genetic scenarios, including: (a) sub-thrust faults within the basement, (b) basement-rooted faults propagating into the sedimentary cover, (c) drape folds overlying basement structures, and (d) linear zones of stratigraphic thickness variation. The TZs observed in the CSA correspond to the second case and partially to the fourth. Structural inheritance is recognized as a key control on the development of TZs, as documented in numerous orogenic systems worldwide, including the Alps (Castellarin et al., 2006; Parizot et al., 2022; Schönborn, 1992;

Schwartz et al., 2024; Zanchi et al., 2012), the Apennines (Satolli et al., 2014), the Pyrenees (Tavani et al., 2013), the Appalachians (Thomas, 1990), the Tasmanides (Glen & Walshe, 1999), the Moine Thrust Belt (Krabbendam & Leslie, 2010), the Wasatch Mountains (Paulsen & Marshak, 1998), the Rocky Mountains (Bégin & Spratt, 2002), the Tian Shan (Rolland et al., 2013), the Zagros (Alavi, 2007) and the Himalaya (Godin et al., 2019). As observed in other belts, our data provide new clues for the syn-orogenic role of TZs and their influence on thrust propagation during continental collision (e.g., Paulsen & Marshak, 1998; Prosser, 1998; Thomas & Bayona, 2002; Zanchi et al., 2012). The combination of our structural and geochronological data provides, to our best knowledge, the first evidence supported by radiometric dating of multiple tectonic reactivations of these structures during both pre-orogenic and syn-orogenic stages (Figures 13 and 14). The episodic reactivation of TZs during orogenic processes suggests that they represent inherited fault systems reactivated at different stages within various tectonic settings, including fold-and-thrust belts. This feature indicates that TZs can act both as inherited, passive structural anisotropies and as persistently reactivated, mechanically weak discontinuities. Owing in part to their typically steep to sub-vertical geometry, they are easily reactivated under changing stress fields, thereby influencing strain partitioning, timing, and structural style over tens of millions of years. Indirect evidence of multiple reactivations of TZs has been documented in both the Alps and other orogenic belts worldwide. In the CSA, Zanchi et al. (2012) reconstructed the tectonic evolution of the Grem–Vedra fault system, spanning from the Late Cretaceous to the Middle Eocene. Castellarin et al. (2006) documented by stratigraphic evidence that the Giudicarie Line was active from the Aptian to the Late Miocene. These cases suggest that TZs may remain mechanically active for nearly the entire duration of an orogenic cycle, undergoing multiple reactivations during different stages of crustal shortening and thrust propagation. Worldwide, repeated reactivations of TZs have also been recognized. Glen and Walshe (1999), for example, documented a prolonged shear history for the Lachlan TZ in southeastern Australia. In Late Ordovician, this fault was a major crustal tear oblique to the convergent margin between the Australian and proto-Pacific plates. Then it was resheared during contractional tectonics in Middle Devonian-Carboniferous times. Thomas (2006) showed that, across multiple Wilson cycles, the same cross-strike structures were repeatedly reactivated, either as syn-orogenic TZs during continental collisions or as transform faults during phases of oceanic opening. These examples highlight not only the structural longevity of TZs as inherited features, but also their functional persistence during compressional (and not only) stages, sometimes spanning time periods of more than 100 million years within the same orogen. In many cases, such structures continue to influence modern deformation patterns and even active faulting, underscoring their geodynamic significance and relevance for seismic hazard assessment (e.g., Carulli & Slejko, 2009; Zampieri et al., 2021). Furthermore, due to their structural complexity and recurrent reactivations, TZs often act as key pathways for the migration of magmatic and hydrothermal fluids. They are important targets for mineral exploration (Bégin & Spratt, 2002; Glen & Walshe, 1999; Summino et al., 2024) and play key roles in controlling subsurface fluid flow relevant to groundwater (Smeraglia et al., 2022) and hydrocarbon reservoirs (Thomas, 2006).

6. Conclusions

Based on stratigraphic, structural and geochronological analyses, this study provides new insights into the origin, syn-orogenic reactivation and tectonic role of TZs of the CSA. The main findings can be summarized as follows:

1. TZs in the CSA developed along inherited stratigraphic–structural discontinuities formed mainly during Late Norian and Early–Middle Jurassic pre-orogenic rifting stages.
2. TZs were reactivated multiple times during the Alpine orogeny, from the Early Cretaceous to the Miocene, consistent with repeated deformation events documented across the belt. Strike-slip and transpressional kinematics observed along these N–S faults are consistent with reactivation under a ca. N–S oriented maximum principal paleostress axis, and with the positive inversion of N-dipping pre-orogenic faults.
3. Within the CSA, TZs influence the belt's 3D architecture by contributing to along-strike strain partitioning, thrust segmentation/merging and shortening accommodation, possibly including vertical-axis rotations and lateral ramping.
4. Our U–Pb data suggest a build-up of the exposed part of the CSA through several phases, including: Cretaceous-Early Eocene (emplacement of thrust sheets 1–2); Eocene-Oligocene (in-sequence build-up of the FP); Late Miocene (synchronous/out-of-sequence reactivation of the FP).

Conflict of Interest

The authors declare no conflicts of interest relevant to this study.

Availability Statement

Structural data shown in this text and the U–Pb data used for constraining the age of syn-tectonic carbonates in this study are available in the EarthChem repository (Fiorini & Kylander-Clark, 2025) with CC-BY-4.0.

Acknowledgments

Funding by MASE (the Italian Ministry of the Environment and Energy Security) to the Earth Science Department-Sapienza Università di Roma and IGAG-CNR for the project "Circolazione di fluidi nelle zone di faglia della Val d'Agri" is acknowledged. MASE is also thanked for allowing publication of the data acquired in the project. This work was also funded by Sapienza Progetti di Ateneo 2023 (E. Carminati), and Avvio alla Ricerca 2024 (A. Fiorini). This study was also carried out within the RETURN Extended Partnership and received funding from the European Union Next-GenerationEU (National Recovery and Resilience Plan—NRRP, Mission 4, Component 2, Investment 1.3—D.D. 1243 2/8/2022, PE0000005). Financial support by the Italian Ministry of University, and Research (MUR) through PRIN project "FAST-Fault architecture in space and time" (PRIN 2020, PI G. Viola; CUP Master J33C22000170001) is acknowledged (L. Aldega and S. Zanchetta). PETEX is acknowledged for the 3D Move licence to the Earth Science Department of Sapienza, University of Rome. Mimmo Mannetta is kindly thanked for preparation of thin sections. Marco Brandano, Diego Marianelli (Sapienza, University of Rome), Stefano M. Bernasconi and Nathan Looser (ETH Zürich) are thanked for assistance with cathodoluminescence analyses. We thank two anonymous reviewers for their constructive comments and suggestions, which greatly improved an earlier version of the manuscript. We thank the editor, Djordje Grujic, for his revisions and careful handling of the paper. Open access publishing facilitated by Universita degli Studi di Roma La Sapienza, as part of the Wiley - CRUI-CARE agreement.

References

Agliardi, F., & Crosta, G. B. (2014). Supporting rockfall countermeasure design in difficult conditions. In *Landslide science for a safer geo-environment: Volume 3: Targeted landslides* (pp. 71–76). Springer International Publishing.

Alavi, M. (2007). Structures of the Zagros fold-thrust belt in Iran. *American Journal of Science*, *307*(9), 1064–1095. https://doi.org/10.2475/09.2007.02

Assereto, R., & Casati, P. (1965). Revisione della stratigrafia permo-triassica della Val Camonica meridionale (Lombardia). *Rivista Italiana di Paleontologia e Stratigrafia*, *71*(4), 999–1097.

Bayona, G., Thomas, W. A., & Van Der Voo, R. (2003). Kinematics of thrust sheets within transverse zones: A structural and paleomagnetic investigation in the Appalachian thrust belt of Georgia and Alabama. *Journal of Structural Geology*, *25*(8), 1193–1212. https://doi.org/10.1016/S0191-8141(02)00162-1

Becker, S., Hilgers, C., Kukla, P. A., & Urai, J. L. (2011). Crack-seal microstructure evolution in bi-mineralic quartz–chlorite veins in shales and siltstones from the RWTH-1 well, Aachen, Germany. *Journal of Structural Geology*, *33*(4), 676–689. https://doi.org/10.1016/j.jsg.2011.01.001

Bégin, N. J., & Spratt, D. A. (2002). Role of transverse faulting in along-strike termination of Limestone Mountain Culmination, Rocky Mountain thrust-and-fold belt, Alberta, Canada. *Journal of Structural Geology*, *24*(4), 689–707. https://doi.org/10.1016/S0191-8141(01)00119-5

Bernoulli, D. (2007). The pre-alpine geodynamic evolution of the Southern Alps: A short summary. *Bulletin Fuer Angewandte Geologie*, *12*, 3–10.

Bernoulli, D., Beckmann, J. P., Bolli, H. M., & Gunzenhauser, B. A. (1987). *Upper Cretaceous deep-water sediments near Prella (Southern Alps, Mendrisiotto, Switzerland)* (Vol. 39, pp. 49–71). Memorie Scienze Geoligiche, Padova.

Bernoulli, D., Bertotti, G., & Zingg, A. (1989). Northward thrusting of the gonfolite Lombarda (South-Alpine molasse) onto the Mesozoic sequence of the lombardian alps: Implications for the deformation history of the Southern alps. Northward thrusting of the gonfolite Lombarda (South-Alpine molasse) onto the Mesozoic sequence of the lombardian alps: Implications for the deformation history of the Southern alps. *Eclogae Geologicae Helvetia*, *82*(3), 841–856. https://doi.org/10.5169/seals-166405

Bernoulli, D., & Winkler, W. (1990). Heavy mineral assemblages from Upper Cretaceous South-and Austroalpine flysch sequences (Northern Italy and Southern Switzerland): Source terranes and palaeotectonic implications. *Eclogae Geologicae Helvetiae*, *83*(2), 287–310.

Berra, F., & Carminati, E. (2010). Subsidence history from a backstripping analysis of the Permo-Mesozoic succession of the Central Southern Alps (Northern Italy). *Basin Research*, *22*(6), 952–975. https://doi.org/10.1111/j.1365-2117.2009.00453.x

Berra, F., Carminati, E., Jadoul, F., & Binda, M. (2016). Does compaction-induced subsidence control accommodation space at the top of prograding carbonate platforms? Constraints from the numerical modelling of the Triassic Esino Limestone (Southern Alps, Italy). *Marine and Petroleum Geology*, *78*, 621–635. https://doi.org/10.1016/j.marpetgeo.2016.09.033

Berra, F., & Jadoul, F. (1996). Norian serpulid and microbial bioconstructions: Implication for the platform evolution in the Lombardy Basin (Southern Alps, Italy). *Facies*, *35*(1), 143–162. https://doi.org/10.1007/BF02536961

Berra, F., & Jadoul, F. (2002). Evidence of a "Mid-Carnian" transgression in the western Southern Alps (Lombardy, Italy): Stratigraphic and paleogeographic implications. *Rivista Italiana di Paleontologia e Stratigrafia*, *108*(1), 119–131.

Berra, F., Jadoul, F., Binda, M., & Lanfranchi, A. (2011). Large-scale progradation, demise and rebirth of a high-relief carbonate platform (Triassic, Lombardy Southern Alps, Italy). *Sedimentary Geology*, *239*(1), 48–63. https://doi.org/10.1016/j.sedgeo.2011.05.002

Bersezio, R., Bini, A., Gelati, R., Ferliga, C., Rigamonti, I., & Strini, A. (2014). *Foglio 097 Vimercate. Note illustrative della Carta Geologica d'Italia alla scala 1:50.000*. ISPRA—Servizio Geologico d'Italia. https://doi.org/10.15161/oar.it/211511

Bersezio, R., Fantoni, R., & Pessina, C. (2001). L'assetto strutturale del margine Sudalpino-padano: Contributo alla conoscenza del sottosuolo nel settore bergamasco. *Geologia Insubrica*, *6*(1), 81–93.

Bersezio, R., & Fornaciari, M. (1987). Cretaceous sequences in the Lombardy Basin: Stratigraphic outline between the lakes of Lecco and Iseo. *Memorie della Societa Geologica Italiana*, *40*, 187–197.

Bersezio, R., Fornaciari, M., Gelati, R., Napolitano, A., & Valdisturlo, A. (1993). The significance of the Upper Cretaceous to Miocene clastic wedges in the deformation history of the Lombardian southern Alps. *Geologie Alpine*, *69*, 3–20.

Bertotti, G. (1991). Early mesozoic extension and Alpine shortening in the western southern Alps: The geology of the area between Lugano and Menaggio (Lombardy, northern Italy). *Memorie di Scienze Geologiche*, *43*, 17–123.

Bertotti, G., Picotti, V., Bernoulli, D., & Castellarin, A. (1993). From rifting to drifting: Tectonic evolution of the South-Alpine upper crust from the Triassic to the Early Cretaceous. *Sedimentary Geology*, *86*(1), 53–76. https://doi.org/10.1016/0037-0738(93)90133-P

Bilau, A., Bienveignant, D., Rolland, Y., Schwartz, S., Godeau, N., Guihou, A., et al. (2023). The Tertiary structuration of the Western Subalpine foreland deciphered by calcite-filled faults and veins. *Earth-Science Reviews*, *236*, 104–270. https://doi.org/10.1016/j.earscirev.2022.104270

Bilau, A., Rolland, Y., Schwartz, S., Gautheron, C., Dumont, T., Bienveignant, D., et al. (2025). Timing of syn-orogenic extension in the Western Alps revealed by calcite U-Pb and hematite (U-Th)/He dating. *Geoscience Frontiers*, *16*(2), 101969. https://doi.org/10.1016/j.gsf.2024.101969

Bini, A., Cita, M. B., & Gaetani, M. (1978). Southern Alpine lakes-Hypothesis of an erosional origin related to the Messinian entrenchment. *Marine Geology*, *27*(3–4), 271–288. https://doi.org/10.1016/0025-3227(78)90035-X

Blom, J. C., & Passchier, C. W. (1997). Structures along the orobic thrust, central orobic alps, Italy. *Geologische Rundschau*, *86*(3), 627–636. https://doi.org/10.1007/s005310050168

Bons, P. D., Elburg, M. A., & Gomez-Rivas, E. (2012). A review of the formation of tectonic veins and their microstructures. *Journal of Structural Geology*, *43*, 33–62. https://doi.org/10.1016/j.jsg.2012.07.005

Boyer, S. E., & Elliott, D. (1982). Thrust systems. *AAPG Bulletin*, *66*(9), 1196–1230. https://doi.org/10.1306/03B5A77D-16D1-11D7-8645000102C1865D

Brack, P., & Rieber, H. (1993). Towards a better definition of the Anisian/Ladinian boundary: New biostratigraphic data and correlations of boundary sections from the Southern Alps. *Eclogae Geologicae Helvetiae*, *86*(2), 415–527. https://doi.org/10.5169/seals-167250
Bresciani, I., & Perotti, C. R. (2014). An active deformation structure in the Po Plain (N Italy): The Romanengo anticline. *Tectonics*, *33*(10), 2059–2076. https://doi.org/10.1002/2013TC003422
Caine, J. S., & Minor, S. A. (2009). Structural and geochemical characteristics of faulted sediments and inferences on the role of water in deformation, Rio Grande Rift, New Mexico. *GSA Bulletin*, *121*(9–10), 1325–1340. https://doi.org/10.1130/B26164.1
Calassou, S., Larroque, C., & Malavieille, J. (1993). Transfer zones of deformation in thrust wedges: An experimental study. *Tectonophysics*, *221*(3), 325–344. https://doi.org/10.1016/0040-1951(93)90165-G
Carminati, E., & Doglioni, C. (2012). Alps vs. Apennines: The paradigm of a tectonically asymmetric Earth. *Earth-Science Reviews*, *112*(1), 67–96. https://doi.org/10.1016/j.earscirev.2012.02.004
Carminati, E., Lustrino, M., Cuffaro, M., & Doglioni, C. (2010). Tectonics, magmatism and geodynamics of Italy: What we know and what we imagine. *Journal of the Virtual Explorer*, *36*(8), 10–3809. https://doi.org/10.3809/jvirtex.2010.00226
Carminati, E., Siletto, G. B., & Battaglia, D. (1997). Thrust kinematics and internal deformation in basement-involved fold and thrust belts: The eastern Orobic Alps case (Central Southern Alps, northern Italy). *Tectonics*, *16*(2), 259–271. https://doi.org/10.1029/96TC03936
Carulli, G. B., & Slejko, D. (2009). Seismotectonic characteristics of the Italian central Alps and implications for the seismic hazard. *Italian Journal of Geosciences*, *128*(1), 201–215.
Casati, P., & Gnaccolini, M. (1967). Geologia delle Alpi Orobie occidentali. Geologia delle Alpi Orobie occidentali. *Rivista Italiana di Paleontologia e Stratigrafia*, *73*, 25–162.
Cassano, E., Anelli, L., Fichera, R., & Cappelli, V. (1986). Pianura Padana: Interpretazione integrata di dati geofisici e geologici. In *Atti del 73° Congresso della Società Geologica Italiana (Roma, 29/09–4/10 1986)*.
Cassinis, G. (1968). *Stratigrafia e tettonica dei terreni mesozoici compresi tra Brescia e Serle* (Vol. 19, pp. 50–152). Atti dell'Istituto di Geologia, Università di Pavia.
Castellarin, A., Cantelli, L., Fesce, A. M., Mercier, J. L., Picotti, V., Pini, G. A., et al. (1992). Alpine compressional tectonics in the Southern Alps. Relationships with the N-Apennines. *Annales Tectonicae*, *6*(1), 62–94.
Castellarin, A., Vai, G. B., & Cantelli, L. (2006). The Alpine evolution of the Southern Alps around the Giudicarie faults: A Late Cretaceous to early Eocene transfer zone. *Tectonophysics*, *414*(1), 203–223. https://doi.org/10.1016/j.tecto.2005.10.019
Ceccato, A., Behr, W. M., Zappone, A. S., Tavazzani, L., & Giuliani, A. (2024). Structural evolution, exhumation rates, and rheology of the European crust during Alpine collision: Constraints from the Rotondo granite-gotthard nappe. *Tectonics*, *43*(6), e2023TC008219. https://doi.org/10.1029/2023TC008219
Curzi, M., Billi, A., Carminati, E., & Tavani, S. (2025). Spatio-temporal constraints on thrusting across fold-and-thrust belts worldwide. *Scientific Reports*, *15*(1), 35642. https://doi.org/10.1038/s41598-025-19660-w
Curzi, M., Viola, G., Zuccari, C., Aldega, L., Billi, A., van der Lelij, R., et al. (2024). Tectonic evolution of the Eastern Southern alps (Italy): A reappraisal from new structural data and geochronological constraints. *Tectonics*, *43*(3), e2023TC008013. https://doi.org/10.1029/2023TC008013
D'Adda, P., Zanchi, A., Bergomi, M., Berra, F., Malusà, M. G., Tunesi, A., & Zanchetta, S. (2011). Polyphase thrusting and dyke emplacement in the central Southern Alps (Northern Italy). *International Journal of Earth Sciences*, *100*(5), 1095–1113. https://doi.org/10.1007/s00531-010-0586-2
Dahlstrom, C. D. (1970). Structural geology in the eastern margin of the Canadian Rocky Mountains. *Bulletin of Canadian Petroleum Geology*, *18*(3), 332–406.
Dal Piaz, G. V., Bistacchi, A., & Massironi, M. (2003). Geological outline of the Alps. *Episodes Journal of International Geoscience*, *26*(3), 175–180. https://doi.org/10.18814/epiiugs/2003/v26i3/004
Delvaux, D., & Sperner, B. (2003). New aspects of tectonic stress inversion with reference to the TENSOR program. *Geological Society, London, Special Publications*, *212*(1), 75–100. https://doi.org/10.1144/GSL.SP.2003.212.01.06
Desio, A. (1929). Studi geologici sulla regione dell'Albenza (Prealpi bergamasche). *Memorie della Societa Italiana di Scienze Naturali e del Museo Civico di Storia Naturale di Milano*, *10*(1), 1–152.
de Sitter, L. U. (1960). *La Structure des Alpes Lombardes. Livrè a la memoire de Prof* (pp. 243–256). P. Fallot-Memoires hors-seriè de la Societè Geologique de. France.
de Sitter, L. U., & de Sitter-Koomans, C. M. (1949). The geology of the Bergamasc Alps, Lombardia, Italy. *Leidse Geologische Mededelingen*, *14*(2), 1–257.
Destro, N. (1995). Release fault: A variety of cross fault in linked extensional fault systems, in the Sergipe-Alagoas Basin, NE Brazil. *Journal of Structural Geology*, *17*(5), 615–629. https://doi.org/10.1016/0191-8141(94)00088-H
Di Giulio, A., Carrapa, B., Fantoni, R., Gorla, L., & Valdisturlo, A. (2001). Middle Eocene to Early Miocene sedimentary evolution of the western Lombardian segment of the South Alpine foredeep (Italy). *International Journal of Earth Sciences*, *90*(3), 534–548. https://doi.org/10.1007/s005310000186
Di Capua, A., Vezzoli, G., & Groppelli, G. (2016). Climatic, tectonic and volcanic controls of sediment supply to an Oligocene Foredeep basin: The Val d'Aveto Formation (Northern Italian Apennines). *Sedimentary Geology*, *332*, 68–84. https://doi.org/10.1016/j.sedgeo.2015.11.009
Doglioni, C., & Bosellini, A. (1987). Eoalpine and mesoalpine tectonics in the Southern Alps. *Geologische Rundschau*, *76*(3), 735–754. https://doi.org/10.1007/BF01821061
Doglioni, C., & Carminati, E. (2008). Structural styles and Dolomites field trip. *Memorie Descrittive della Carta Geologica d'Italia*, *82*, 1–296.
Faccenna, C., Mattei, M., Funiciello, R., & Jolivet, L. (1997). Styles of back-arc extension in the central Mediterranean. *Terra Nova*, *9*(3), 126–130. https://doi.org/10.1046/j.1365-3121.1997.d01-12.x
Fantoni, R., Bersezio, R., & Forcella, F. (2004). Alpine structure and deformation chronology at the southern Alps-Po Plain border in Lombardy. *Bollettino della Societa Geologica Italiana*, *123*(3), 463–476.
Feriozzi, F., Siravo, G., & Speranza, F. (2025). Heritage of Tethyan oceanic transform faults within Alpine orogens: Paleomagnetic evidence from theShkoder-Peja transverse zone (northern Albania). *Tectonics*, *44*(6), e2024TC008743. https://doi.org/10.1029/2024TC008743
Fiorini, A., & Kylander-Clark, A. (2025). U-Pb dating of calcite mineralizations and Mesostructural data collected in the Central Southern Alps, Lecco Area (Lombardy, Italy). [Dataset] version 1.0. *Interdisciplinary Earth Data Alliance (IEDA)*. https://doi.org/10.60520/IEDA/114132
Forcella, F., Jadoul, F., Bini, A., Ferliga, C., Rossi, S., & Piccin, A. (2000). Carta geologica della Provincia di Bergamo alla scala 1:50.000 con relativa nota illustrativa. In *Provincia di Bergamo, 1-313, 3 cartographic sheets*.
Gaetani, M., Gnaccolini, M., Poliani, G., Grignani, D., Gorza, M., & Martellini, L. (1991). An anoxic intraplatform basin in the Middle Triassic of Lombardy (Southern Alps, Italy): Anatomy of a hydrocarbon source. *Rivista Italiana di Paleontologia e Stratigrafia*, *97*(3–4). https://doi.org/10.13130/2039-4942/8954

Gaetani, M., Sciunnach, D., Bini, A., & Rossi, S. (2012). *Foglio 076 Lecco. Note illustrative della Carta Geologica d'Italia alla scala 1:50.000* (pp. 1–216). ISPRA—Servizio Geologico d'Italia.

García, H., & Jiménez, G. (2016). Transverse zones controlling the structural evolution of the Zipaquira Anticline (Eastern Cordillera, Colombia): Regional implications. *Journal of South American Earth Sciences*, *69*, 243–258. https://doi.org/10.1016/j.jsames.2016.04.002

Garzanti, E., Gnaccolini, M., & Jadoul, F. (1995). Anatomy of a semiarid coastal system: The upper Carnian of Lombardy (Italy). *Rivista Italiana di Paleontologia e Stratigrafia*, *101*(1), 1736.

Gianotti, R. (1984). Osservazioni in merito ad una attività triassica della Linea Orobica in prossimità del Lago di Como. Osservazioni in Merito Ad Una Attività Triassica Della Linea Orobica in Prossimità Del Lago Di Como. *Rendiconti della Societa Geologica Italiana*, *7*, 9–10.

Gianotti, R., & Perotti, C. R. (1986). Introduzione alla tettonica e all'evoluzione strutturale delle Alpi Lariane. *Memorie della Societa Geologica Italiana*, *32*, 67–99.

Glen, R. A., & Walshe, J. L. (1999). Cross-structures in the lachlan orogen: The lachlan transverse Zone example. *Australian Journal of Earth Sciences*, *46*(4), 641–658. https://doi.org/10.1046/j.1440-0952.1999.00734.x

Godin, L., Soucy La Roche, R., Waffle, L., & Harris, L. B. (2019). Influence of inherited Indian basement faults on the evolution of the Himalayan Orogen. *Geological Society, London, Special Publications*, *481*(1), 251–276. https://doi.org/10.1144/SP481.4

Handy, M. R., Schmid, S. M., Bousquet, R., Kissling, E., & Bernoulli, D. (2010). Reconciling plate-tectonic reconstructions of Alpine Tethys with the geological–geophysical record of spreading and subduction in the Alps. *Earth-Science Reviews*, *102*(3–4), 121–158. https://doi.org/10.1016/j.earscirev.2010.06.002

Jadoul, F. (1994). Middle Triassic stratigraphy and paleogeography of the Muschiada tectonic unit: Structural implications for the Valsassina domain (Southern Alps, Lombardy). *Quaderni Di Geodinamica Alpina e Quaternaria*, *2*, 145–160.

Jadoul, F., Berra, F., & Frisia, S. (1992). Stratigraphic and paleogeographic evolution of a carbonate platform in an extensional tectonic regime: The example of the Dolomia Principale in Lombardy (Italy). *Rivista Italiana di Paleontologia e Stratigrafia*, *98*(1). https://doi.org/10.13130/2039-4942/8939

Jadoul, F., & Doniselli, T. (1986). La successione del Lias inferiore di Morterone (Lecchese). *Memorie della Societa Geologica Italiana*, *32*, 49–66.

Jadoul, F., & Gaetani, M. (1986). L'assetto strutturale del settore Lariano centro-meridionale. *Memorie della Societa Geologica Italiana*, *32*, 123–131.

Krabbendam, M., & Leslie, A. G. (2010). Lateral variations and linkages in thrust geometry: The Traligill Transverse Zone, Assynt Culmination, Moine Thrust Belt, NW Scotland. *Geological Society, London, Special Publications*, *335*(1), 335–357. https://doi.org/10.1144/SP335.16

Kylander-Clark, A. R. (2020). Expanding the limits of laser-ablation U–Pb calcite geochronology. *Geochronology*, *2*(2), 343–354. https://doi.org/10.5194/gchron-2-343-2020

Laubscher, H. P. (1985). Large-scale, thin-skinned thrusting in the southern Alps: Kinematic models. *Geological Society of America Bulletin*, *96*(6), 710–718. https://doi.org/10.1130/0016-7606(1985)96<710:LTTITS>2.0.CO;2

Le Breton, E., Handy, M. R., Molli, G., & Ustaszewski, K. (2017). Post-20 Ma motion of the Adriatic Plate: New constraints from surrounding orogens and implications for crust-mantle decoupling. *Tectonics*, *36*(12), 3135–3154. https://doi.org/10.1002/2016TC004443

Lescoutre, R., Manatschal, G., & Muñoz, J. A. (2021). Nature, origin, and evolution of the Pyrenean-Cantabrian junction. *Tectonics*, *40*(5), e2020TC006134. https://doi.org/10.1029/2020TC006134

Locchi, S., Zanchetta, S., & Zanchi, A. (2022). Evidence of early Permian extension during the Post-Variscan evolution of the central Southern Alps (N Italy). *International Journal of Earth Sciences*, *111*(6), 1717–1738. https://doi.org/10.1007/s00531-022-02220-2

Looser, N., Madritsch, H., Guillong, M., Laurent, O., Wohlwend, S., & Bernasconi, S. M. (2021). Absolute age and temperature constraints on deformation along the basal décollement of the Jura fold-and-thrust belt from carbonate U-Pb dating and clumped isotopes. *Tectonics*, *40*(3), e2020TC006439. https://doi.org/10.1029/2020TC006439

Luo, K., Zhou, J.-X., Feng, Y.-X., Uysal, I. T., Nguyen, A., Zhao, J.-X., & Zhang, J. (2020). In situ U-Pb dating of calcite from the south China antimony metallogenic Belt. *iScience*, *23*(10), 101575. https://doi.org/10.1016/j.isci.2020.101575

Malekzade, Z., Bellier, O., Abbassi, M. R., Shabanian, E., & Authemayou, C. (2016). The effects of plate margin inhomogeneity on the deformation pattern within west-Central Zagros fold-and-thrust Belt. *Tectonophysics*, *693*, 304–326. https://doi.org/10.1016/j.tecto.2016.01.030

Mazzoli, S., Basilici, M., Spina, V., Pierantoni, P. P., & Tondi, E. (2022). Space and time variability of detachment-versus ramp-dominated thrusting: Insights from the outer Albanides. *Tectonics*, *41*(8), e2022TC007274. https://doi.org/10.1029/2022TC007274

Michetti, A., Livio, F., Vezzoli, L., Pasquaré Mariotto, F., Brunamonte, F., Berlusconi, A., et al. (2012). Foglio 075 Como. In *Note illustrative della Carta Geologica d'Italia alla scala 1:50000*.

Parizot, O., Missenard, Y., Barbarand, J., Blaise, T., Benedicto, A., Haurine, F., & Sarda, P. (2022). How sensitive are intraplate inherited structures? Insight from the Cévennes Fault System (Languedoc, SE France). *Geological Magazine*, *159*(11–12), 2082–2094. https://doi.org/10.1017/S0016756822000152

Paulsen, T., & Marshak, S. (1998). Charleston transverse zone, Wasatch Mountains, Utah: Structure of the Provo salient's northern margin, Sevier fold-thrust belt. *GSA Bulletin*, *110*(4), 512–522. https://doi.org/10.1130/0016-7606(1998)110<0512:CTZWMU>2.3.CO;2

Paulsen, T., & Marshak, S. (1999). Origin of the Uinta recess, Sevier fold–thrust belt, Utah: Influence of basin architecture on fold–thrust belt geometry. *Tectonophysics*, *312*(2), 203–216. https://doi.org/10.1016/S0040-1951(99)00182-1

Peacock, D. C., Tavarnelli, E., & Anderson, M. W. (2017). Interplay between stress permutations and overpressure to cause strike-slip faulting during tectonic inversion. *Terra Nova*, *29*(1), 61–70. https://doi.org/10.1111/ter.12249

Picotti, V., Prosser, G., & Castellarin, A. (1995). Kinematics of the Giudicarie-Valtrompia fold and thrust belt (Central Southern Alps, Northern Italy). *Memorie di Scienze Geologiche*, *47*, 95–109.

Pieri, M., & Groppi, G. (1981). *Subsurface geological structure of the Po plain, Italy* (Vol. 414). Progetto Finalizzato Geodinamica C.N.R. https://doi.org/10.13140/RG.2.1.4945.3840

Pleuger, J., Mancktelow, N., Zwingmann, H., & Manser, M. (2012). K–Ar dating of synkinematic clay gouges from Neoalpine faults of the Central, Western and Eastern Alps. *Tectonophysics*, *550*, 1–16. https://doi.org/10.1016/j.tecto.2012.05.001

Pohl, F., Froitzheim, N., Obermüller, G., Tomaschek, F., Schröder, O., Nagel, T. J., et al. (2018). Kinematics and Age of syn-intrusive detachment faulting in the Southern alps: Evidence for early Permian crustal extension and implications for the pangea A versus B controversy. *Tectonics*, *37*(10), 3668–3689. https://doi.org/10.1029/2018TC004974

Pomella, H., Stipp, M., & Fügenschuh, B. (2012). Thermochronological record of thrusting and strike-slip faulting along the Giudicarie fault system (Alps, Northern Italy). *Tectonophysics*, *579*, 118–130. https://doi.org/10.1016/j.tecto.2012.04.015

Prosser, G. (1998). Strike-slip movements and thrusting along a transpressive fault zone: The North Giudicarie line (Insubric line, northern Italy). *Tectonics*, *17*(6), 921–937. https://doi.org/10.1029/1998TC900010

Qayyum, M., Spratt, D. A., Dixon, J. M., & Lawrence, R. D. (2015). Displacement transfer from fault-bend to fault-propagation fold geometry: An example from the Himalayan thrust front. *Journal of Structural Geology*, *77*, 260–276. https://doi.org/10.1016/j.jsg.2014.10.010

Ratschbacher, L. (1986). Kinematics of Austro-Alpine cover nappes: Changing translation path due to transpression. *Tectonophysics*, *125*(4), 335–356. https://doi.org/10.1016/0040-1951(86)90170-8

Regione Lombardia. (2010). Carta Geologica della Provincia di Lecco, Scala 1:25000. In *Regione Lombardia – D.G. Territorio e Urbanistica, in collaboration with Provincia di Lecco and Progetto CARG (Nuova Carta Geologica d'Italia)*.

Renard, F., Gratier, J. P., & Jamtveit, B. (2000). Kinetics of crack-sealing, intergranular pressure solution, and compaction around active faults. *Journal of Structural Geology*, *22*(10), 1395–1407. https://doi.org/10.1016/S0191-8141(00)00064-X

Roberts, N. M. W., & Holdsworth, R. E. (2022). Timescales of faulting through calcite geochronology: A review. *Journal of Structural Geology*, *158*, 104578. https://doi.org/10.1016/j.jsg.2022.104578

Rocca, M., Zanchetta, S., Gasparrini, M., Mangenot, X., Berra, F., Deschamps, P., et al. (2024). U-Pb carbonate dating reveals long-lived activity of proximal margin extensional faults during the Alpine Tethys rifting. *Terra Nova*, *36*(5), 347–357. https://doi.org/10.1111/ter.12717

Rocca, M., Zanchetta, S., & Zanchi, A. (2026). Inherited rift faults as drivers of orogenic complexity: The case of the Amora Fault System, central Southern alps (N Italy). *Journal of Structural Geology*. https://doi.org/10.1016/j.jsg.2026.105650e

Roeder, D. (1992). Thrusting and wedge growth, Southern Alps of Lombardia (Italy). *Tectonophysics*, *207*(1), 199–243. https://doi.org/10.1016/0040-1951(92)90478-O

Rolland, Y., Alexeiev, D. V., Kröner, A., Corsini, M., Loury, C., & Monié, P. (2013). Late Palaeozoic to Mesozoic kinematic history of Talas-Ferghana strike-slip Fault (Kyrgyz West Tianshan) revealed by a structural study and 40Ar/39Ar dating. *Journal of Asian Earth Sciences*, *67/68*, 76–92. https://doi.org/10.1016/j.jseaes.2013.02.012

Rolland, Y., Bilau, A., Cardinal, T., Nouibat, A., Bienveignant, D., Boschetti, L., et al. (2022). Bridging the gap between long–term orogenic evolution (>10 Ma Scale) and geomorphological processes that shape the Western Alps: Insights from combined dating approaches. *Geosciences*, *12*(11), 393. https://doi.org/10.3390/geosciences12110393

Rolland, Y., Cox, S. F., & Corsini, M. (2009). Constraining deformation stages in brittle–ductile shear zones from combined field mapping and $^{40}Ar/^{39}Ar$ dating: The structural evolution of the Grimsel Pass area (Aar Massif, Swiss Alps). *Journal of Structural Geology*, *31*(11), 1377–1394. https://doi.org/10.1016/j.jsg.2009.08.003

Rožič, B. (2005). Albian-Cenomanian resedimented limestone in the lower flyschoid formation of the Mt. Mrzli Vrh Area (Tolmin region, NW Slovenia). *Geologija*, *48*(2), 193–210. https://doi.org/10.5474/geologija.2005.017

Santantonio, M., & Carminati, E. (2011). Jurassic rifting evolution of the Apennines and Southern Alps (Italy): Parallels and differences. *GSA Bulletin*, *123*(3–4), 468–484. https://doi.org/10.1130/B30104.1

Satolli, S., Pace, P., Viandante, M. G., & Calamita, F. (2014). Lateral variations in tectonic style across cross-strike discontinuities: An example from the Central Apennines belt (Italy). *International Journal of Earth Sciences*, *103*(8), 2301–2313. https://doi.org/10.1007/s00531-014-1052-3

Schaltegger, U., & Brack, P. (2007). Crustal-scale magmatic systems during intracontinental strike-slip tectonics: U, Pb and Hf isotopic constraints from Permian magmatic rocks of the Southern Alps. *International Journal of Earth Sciences*, *96*(6), 1131–1151. https://doi.org/10.1007/s00531-006-0165-8

Schmid, S. M., Aebli, H. R., Heller, F., & Zingg, A. (1989). The role of the Periadriatic Line in the tectonic evolution of the Alps. *Geological Society, London, Special Publications*, *45*(1), 153–171. https://doi.org/10.1144/GSL.SP.1989.045.01.08

Schmid, S. M., Fügenschuh, B., Kissling, E., & Schuster, R. (2004). Tectonic map and overall architecture of the Alpine orogen. *Eclogae Geologicae Helvetiae*, *97*(1), 93–117. https://doi.org/10.1007/s00015-004-1113-x

Schmid, S. M., Pfiffner, O. A., Froitzheim, N., Schönborn, G., & Kissling, E. (1996). Geophysical-geological transect and tectonic evolution of the Swiss-Italian Alps. *Tectonics*, *15*(5), 1036–1064. https://doi.org/10.1029/96TC00433

Schmidt, C. J., & O'Neill, J. M. (1982). Structural evolution of the Southwest Montana transverse Zone. In R. B. Powers (Ed.), *Geologic studies of the Cordilleran thrust Belt* (Vol. 1, pp. 193–218). Rocky Mountain Association of Geologist.

Schönborn, G. (1992). Alpine tectonics and kinematic models of the Central Southern Alps. *Memorie di Scienze Geologiche*, *44*, 229–393.

Schumacher, M. E., Schönborn, G., Bernoulli, D., & Laubscher, H. P. (1997). Rifting and collision in the southern Alps. In O. A. Pfiffner, P. Lehner, P. Heitzmann, S. Mueller, & A. Steck, et al. (Eds.), *Deep structure of the Swiss Alps. The National Research Program 20 (NRP/20)* (pp. 186–204). Birkhauser Verlag.

Schwartz, S., Rolland, Y., Nouibat, A., Boschetti, L., Bienveignant, D., Dumont, T., et al. (2024). Role of mantle indentation in collisional deformation evidenced by deep geophysical imaging of Western Alps. *Communications Earth & Environment*, *5*(1), 17. https://doi.org/10.1038/s43247-023-01180-y

Sibley, D. F., & Gregg, J. M. (1987). Classification of dolomite rock textures. *Journal of Sedimentary Research*, *57*(6), 967–975. https://doi.org/10.1306/212f8cba-2b24-11d7-8648000102c1865d

Smeraglia, L., Bernasconi, S. M., Berra, F., Billi, A., Boschi, C., Caracausi, A., et al. (2018). Crustal-scale fluid circulation and co-seismic shallow comb-veining along the longest normal fault of the central Apennines, Italy. *Earth and Planetary Science Letters*, *498*, 152–168. https://doi.org/10.1016/j.epsl.2018.06.013

Smeraglia, L., Fabbri, O., Choulet, F., Jaggi, M., & Bernasconi, S. M. (2022). The role of thrust and strike-slip faults in controlling regional-scale paleofluid circulation in fold-and-thrust belts: Insights from the Jura Mountains (eastern France). *Tectonophysics*, *829*, 229299. https://doi.org/10.1016/j.tecto.2022.229299

Smeraglia, L., Looser, N., Fabbri, O., Choulet, F., Guillong, M., & Bernasconi, S. M. (2021). U–Pb dating of middle Eocene–Pliocene repeated tectonic pulses in the Alpine foreland. *Solid Earth*, *12*(11), 2539–2551. https://doi.org/10.5194/se-12-2539-2021

Soto, R., Casas, A. M., Storti, F., & Faccenna, C. (2002). Role of lateral thickness variations on the development of oblique structures at the Western end of the South Pyrenean Central Unit. *Tectonophysics*, *350*(3), 215–235. https://doi.org/10.1016/S0040-1951(02)00116-6

Summino, L., Domenighini, G., Giorno, M., Barale, L., Bertok, C., Martire, L., et al. (2024). Geology of the Arera-Vedra Valley mining area (Gorno district, Orobic Alps, Italy). *Journal of Maps*, *20*(1), 2422545. https://doi.org/10.1080/17445647.2024.2422545

Tavani, S., Carola, E., Granado, P., Quintà, A., & Muñoz, J. A. (2013). Transpressive inversion of a Mesozoic extensional forced fold system with an intermediate décollement level in the Basque-Cantabrian Basin (Spain). *Tectonics*, *32*(2), 146–158. https://doi.org/10.1002/tect.20019

Tavani, S., Storti, F., Lacombe, O., Corradetti, A., Muñoz, J. A., & Mazzoli, S. (2015). A review of deformation pattern templates in foreland basin systems and fold-and-thrust belts: Implications for the state of stress in the frontal regions of thrust wedges. *Earth-Science Reviews*, *141*, 82–104. https://doi.org/10.1016/j.earscirev.2014.11.013

Thomas, W. A. (1990). Controls on locations of transverse zones in thrust belts. *Eclogae Geologicae Helvetiae*, *83*(3), 727. https://doi.org/10.5169/seals-166611

Thomas, W. A. (2006). Tectonic inheritance at a continental margin. *GSA Today*, *16*(2), 4–11. https://doi.org/10.1130/1052-5173(2006)016[4:tiaacm]2.0.co;2

Thomas, W. A., & Bayona, G. (2002). Palinspastic restoration of the Anniston transverse zone in the Appalachian thrust belt, Alabama. *Journal of Structural Geology*, *24*(4), 797–826. https://doi.org/10.1016/S0191-8141(01)00117-1

Tillberg, M., Drake, H., Zack, T., Kooijman, E., Whitehouse, M. J., & Åström, M. E. (2020). In situ Rb-Sr dating of slickenfibres in deep crystalline basement faults. *Scientific Reports*, *10*(1), 562. https://doi.org/10.1038/s41598-019-57262-5

Torres Carbonell, P. J., Dimieri, L. V., & Olivero, E. B. (2013). Evaluation of strain and structural style variations along the strike of the Fuegian thrust-fold belt front, Argentina. *Andean Geology*, *40*(3), 438–457. https://doi.org/10.5027/andgeoV40n3-a03

Toscani, G., Di Bucci, D., Ravaglia, A., Seno, S., Fracassi, U., & Valensise, G. (2009). Propagation of an inherited strike-slip fault through a foreland-chain system: Quantitative aspects from analogue modeling and applications. *Bollettino della Societa Geologica Italiana*, *128*(1), 107–122.

Ustaszewski, K., & Schmid, S. M. (2006). Control of preexisting faults on geometry and kinematics in the northernmost part of the Jura fold-and-thrust belt. *Tectonics*, *25*(5). https://doi.org/10.1029/2005TC001915

Verwater, V. F., Le Breton, E., Handy, M. R., Picotti, V., Jozi Najafabadi, A., & Haberland, C. (2021). Neogene kinematics of the Giudicarie Belt and eastern Southern Alpine orogenic front (northern Italy). *Solid Earth*, *12*(6), 1309–1334. https://doi.org/10.5194/se-12-1309-2021

Viola, G., Mancktelow, N. S., & Seward, D. (2001). Late Oligocene-Neogene evolution of Europe-Adria collision: New structural and geochronological evidence from the Giudicarie fault system (Italian Eastern Alps). *Tectonics*, *20*(6), 999–1020. https://doi.org/10.1029/2001TC900021

Virgo, S., Abe, S., & Urai, J. L. (2014). The evolution of crack seal vein and fracture networks in an evolving stress field: Insights from Discrete Element Models of fracture sealing. *Journal of Geophysical Research: Solid Earth*, *119*(12), 8708–8727. https://doi.org/10.1002/2014JB011520

Vollmer, F. W. (2015). Orient 3: A new integrated software program for orientation data analysis, kinematic analysis, spherical projections, and Schmidt plots. In *Geological Society of America abstracts with programs* (Vol. 47, p. 49).

Walker, J. D., Tikoff, B., Newman, J., Clark, R., Ash, J., Good, J., et al. (2019). StraboSpot data system for structural geology. *Geosphere*, *15*(2), 533–547. https://doi.org/10.1130/GES02039.1

Woodward, N. B., Walker, K. R., & Lutz, C. T. (1988). Relationships between early Paleozoic facies patterns and structural trends in the Saltville thrust family, Tennessee Valley and Ridge, southern Appalachians. *GSA Bulletin*, *100*(11), 1758–1769. https://doi.org/10.1130/0016-7606(1988)100<1758:RBEPFP>2.3.CO;2

Zampieri, D. (2000). Segmentation and linkage of the Lessini Mountains normal faults, Southern Alps, Italy. *Tectonophysics*, *319*(1), 19–31. https://doi.org/10.1016/S0040-1951(00)00025-1

Zampieri, D., Vannoli, P., & Burrato, P. (2021). Geodynamic and seismotectonic model of a long-lived transverse structure: The Schio-Vicenza Fault System (NE Italy). *Solid Earth*, *12*(8), 1967–1986. https://doi.org/10.5194/se-12-1967-2021

Zanchetta, S., D'Adda, P., Zanchi, A., Barberini, V., & Villa, I. M. (2011). Cretaceous-Eocene compression in the central Southern Alps (N Italy) inferred from 40Ar/39Ar dating of pseudotachylytes along regional thrust faults. *Journal of Geodynamics*, *51*(4), 245–263. https://doi.org/10.1016/j.jog.2010.09.004

Zanchetta, S., Garzanti, E., Doglioni, C., & Zanchi, A. (2012). The Alps in the Cretaceous: A doubly vergent pre-collisional orogen. *Terra Nova*, *24*(5), 351–356. https://doi.org/10.1111/j.1365-3121.2012.01071.x

Zanchetta, S., Malusà, M. G., & Zanchi, A. (2015). Precollisional development and Cenozoic evolution of the Southalpine retrobelt (European Alps). *Lithosphere*, *7*(6), 662–681. https://doi.org/10.1130/L466.1

Zanchi, A., Chiesa, S., & Gillot, P.-Y. (1990). Tectonic evolution of the Southern Alps in the Orobic Chain: Structural and geochronological indicators for pre-tertiary compressive tectonics. *Memorie della Societa Geologica Italiana*, *45*, 77–82.

Zanchi, A., D'Adda, P., Zanchetta, S., & Berra, F. (2012). Syn-thrust deformation across a transverse zone: The Grem–Vedra fault system (central Southern Alps, N Italy). *Swiss Journal of Geosciences*, *105*(1), 19–38. https://doi.org/10.1007/s00015-011-0089-6

Zanchi, A., Forcella, F., Jadoul, F., Bernini, M., Bersezio, R., Fornaciari, M., et al. (1988). The Faggio-Morterone transverse line: Mesoscopic analysis and kinematic implications. *Rendiconti della Societa Geologica Italiana*, *11*(2), 279–286.

Zanchi, A., Ravazzi, C., Cavallin, A., Deaddis, M., Amicis, M. D., Arosio, T., et al. (2022). Interplay of Holocene surface faulting and climate in the Central Po Plain, Italy. *Quaternary Research*, *107*, 71–86. https://doi.org/10.1017/qua.2021.68

Zanchi, A., Zanchetta, S., Berio, L., Berra, F., Felletti, F., Volpi, V., et al. (2019). Low-angle normal faults record early Permian extensional tectonics in the Orobic Basin (Southern Alps, N Italy). *Italian Journal of Geosciences*, *138*(2), 184–201. https://doi.org/10.3301/IJG.2018.35

Zattin, M., Cuman, A., Fantoni, R., Martin, S., Scotti, P., & Stefani, C. (2006). From Middle Jurassic heating to Neogene cooling: The thermochronological evolution of the southern Alps. *Tectonophysics*, *414*(1–4), 191–202. https://doi.org/10.1016/j.tecto.2005.10.020

References From the Supporting Information

Hill, C. A., Polyak, V. J., Asmerom, Y., & P. Provencio, P. C. T. C. (2016). Constraints on a Late Cretaceous uplift, denudation, and incision of the Grand Canyon region, southwestern Colorado Plateau, USA, from U-Pb dating of lacustrine limestone. *Tectonics*, *35*(4), 896–906. https://doi.org/10.1002/2016tc004166

Mitra, S., & Mount, V. S. (1998). Foreland basement-involved structures. *AAPG Bulletin*, *82*(1), 70–109. https://doi.org/10.1306/1D9BC39F-172D-11D7-8645000102C1865D

Mitra, S., & Miller, J. F. (2013). Strain variation with progressive deformation in basement-involved trishear structures. *Journal of Structural Geology*, *53*, 70–79. https://doi.org/10.1016/j.jsg.2013.05.007

Nuriel, P., Wotzlaw, J. F., Ovtcharova, M., Vaks, A., Stremtan, C., Šala, M., et al. (2021). The use of ASH-15 flowstone as a matrix-matched reference material for laser-ablation U-Pb geochronology of calcite. *Geochronology*, *3*(1), 35–47. https://doi.org/10.5194/gchron-3-35-2021

Pagel, M., Bonifacie, M., Schneider, D. A., Gautheron, C., Brigaud, B., Calmels, D., et al. (2018). Improving paleohydrological and diagenetic reconstructions in calcite veins and breccia of a sedimentary basin by combining Δ47 temperature, δ18Owater and U-Pb age (2018). *Chemical Geology*, *481*, 1–17. https://doi.org/10.1016/j.chemgeo.2017.12.026

Paton, C., Hellstrom, J., Paul, B., Woodhead, J., & Hergt, J. (2011). Iolite: Freeware for the visualisation and processing of mass spectrometric data. *J Anal Atom Spectom*, *26*(12), 2508–2518. https://doi.org/10.1039/c1ja10172b

Roberts, N. M. W., Rasbury, E. T., Parrish, R. R., Smith, C. J., Horstwood, M. S. A., & Condon, D. J. (2017). A calcite reference material for LA-ICP-MS U-Pb geochronology. *Geochemistry, Geophysics, Geosystems*, *18*(7), 2807–2814. https://doi.org/10.1002/2016GC006784

Vermeesch, P. (2018). IsoplotR: A free and open toolbox for geochronology. *Geoscience Frontiers*, *9*(5), 1479–1493. https://doi.org/10.1016/j.gsf.2018.04.001